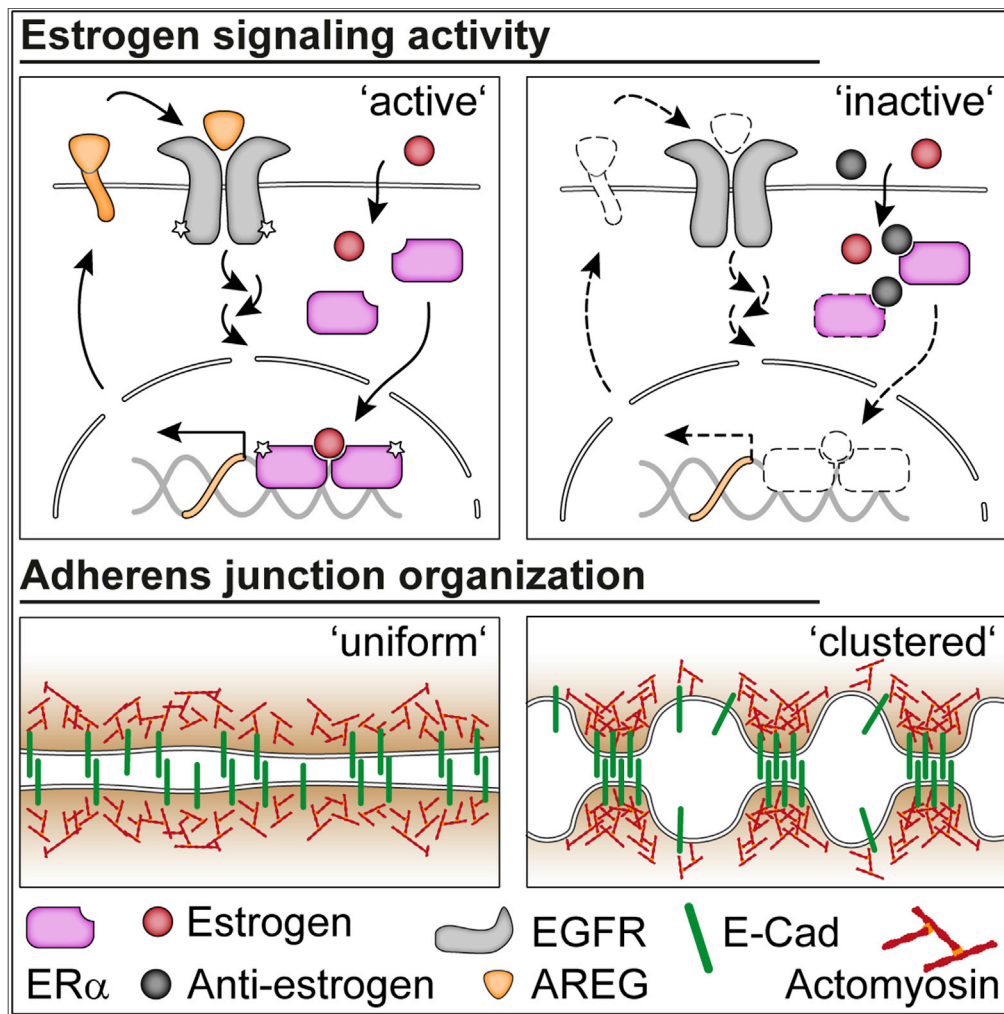**Article**

Estrogens Determine Adherens Junction Organization and E-Cadherin Clustering in Breast Cancer Cells via Amphiregulin

Philip Bischoff, Marja Kornhuber, Sebastian Dunst, ..., Jochen Guck, Michael Oelgeschläger, Gilbert Schönfelder

gilbert.schoenfelder@bfr.bund.de

HIGHLIGHTS

ERα inhibition causes adherens junction (AJ) reorganization through AREG and EGFR

AJ reorganization coincides with microclustering of E-Cadherin at cell membranes

AJ reorganization and microclustering of E-Cadherin are actomyosin dependent

AJ reorganization correlates with increased cell stiffness and reduced motility

iScience

Article

Estrogens Determine Adherens Junction Organization and E-Cadherin Clustering in Breast Cancer Cells via Amphiregulin

Philip Bischoff,[1,2,7] Marja Kornhuber,[1,3,7] Sebastian Dunst,[1] Jakob Zell,[1,2] Beatrix Fauler,[4] Thorsten Mielke,[4] Anna V. Taubenberger,[5] Jochen Guck,[6] Michael Oelgeschläger,[1] and Gilbert Schönfelder[1,2,8,*]

SUMMARY

Estrogens play an important role in the development and progression of human cancers, particularly in breast cancer. Breast cancer progression depends on the malignant destabilization of adherens junctions (AJs) and disruption of tissue integrity. We found that estrogen receptor alpha (ERα) inhibition led to a striking spatial reorganization of AJs and microclustering of E-Cadherin (E-Cad) in the cell membrane of breast cancer cells. This resulted in increased stability of AJs and cell stiffness and a reduction of cell motility. These effects were actomyosin-dependent and reversible by estrogens. Detailed investigations showed that the ERα target gene and epidermal growth factor receptor (EGFR) ligand Amphiregulin (AREG) essentially regulates AJ reorganization and E-Cad microclustering. Our results not only describe a biological mechanism for the organization of AJs and the modulation of mechanical properties of cells but also provide a new perspective on how estrogens and anti-estrogens might influence the formation of breast tumors.

INTRODUCTION

Endogenous estrogens take over various physiological effects in the body, especially in females (Liang and Shang, 2013). Despite these normal physiological effects, not only endogenous but also exogenously supplied estrogens may be associated with the increased incidence of certain cancers, especially breast and endometrial cancers (Liang and Shang, 2013). Breast cancer is the most frequent cancer and the leading cause of cancer death in women worldwide (Wild et al., 2020). Exposure to estrogens and signaling through estrogen receptors are important determinants for breast cancer development and progression (Huang et al., 2014; Thomas and Gustafsson, 2011; Yager and Davidson, 2006). Therefore, inhibitors for estrogen receptor alpha (ERα) such as Tamoxifen (Early Breast Cancer Trialists' Collaborative Group (EBCTCG) et al., 2011; Maximov et al., 2013) and Fulvestrant (Lee et al., 2017) are frequently used during endocrine therapy to prevent breast cancer metastasis. Moreover, exposure to exogenous substances that mimic the action of endogenous estrogen, so-called xenoestrogens, can also stimulate breast tumorigenesis. This has been illustrated by the increased lifetime risk of a broad spectrum of adverse health outcomes including breast cancer in mothers and daughters that were exposed to the synthetic estrogen diethylstilbestrol (DES), when prescribed during pregnancy to prevent miscarriage (Herbst et al., 1971; Hoover et al., 2011).

The process of breast cancer development and progression is an example of a complex disease with diverse responses to hormones. Most metastatic breast cancers are ERα-positive invasive ductal carcinomas (IDCs) (also termed invasive carcinoma of no special type) that emerge in a stepwise fashion from the mammary epithelium lining the lactiferous duct (Wellings and Jensen, 1973). Metastatic breast cancer progression is characterized by the loss of tissue integrity mimicking the developmental epithelial-to-mesenchymal transition (EMT) program (Ye and Weinberg, 2015). Adherens junctions (AJs) essentially regulate tissue integrity and cell dynamics. Thus, individual breast cancer development and progression were shown to depend on the malignant destabilization of AJs and the disruption of cell-cell adhesion. These processes have primarily been attributed to the loss of the essential AJ protein E-Cadherin (E-Cad) (Berx and van Roy, 2009). Although this would provide an easy and intuitive explanation for a mechanism leading to breast cancer cell invasion, E-Cad expression is sustained in most metastasizing IDCs

in vivo (Hashizume et al., 1996; Qureshi et al., 2006). Hence, these data indicate that additional mechanisms influencing AJs exist that underlie the effects of estrogens in ERα-positive/E-Cad-positive types of breast cancer.

Here, we studied the spatial organization and stability of AJs and clustering of E-Cad in the cell membrane under the influence of estrogens and anti-estrogens using the human estrogen-responsive IDC breast cell line MCF-7. We conducted a series of investigations to determine the functional consequences of a spatial reorganization of AJ and microclustering of E-Cad in the cell membrane. Furthermore, we elucidated estrogen-dependent influences on the biomechanical properties of cells and a potential cross talk with the EGFR signaling pathway. In order to evaluate how the estrogen-dependent organization of AJs in breast cancer cells translates into a clinical setting, we tested whether comparable effects could also be observed in breast tumor tissue samples.

RESULTS

Estrogen Signaling Controls Organization of Adherens Junctions

Inhibition of ERα Signaling Results in a Striking Spatial Reorganization of Adherens Junctions

To expand the mechanistic understanding of estrogen signaling in breast cancer, we treated human ERα-positive/E-Cad-positive MCF-7 breast cancer cells with the potent anti-estrogen Fulvestrant (Fulv) at clinically relevant concentrations in the nanomolar range (McCormack and Sapunar, 2008) and analyzed the morphology of cell-cell contacts in confluent monolayers. We found that Fulv-mediated inhibition of ERα signaling resulted in a striking spatial reorganization of the cell-cell contact region at the level of the zonula adherens (Figure 1A). Although AJs (visualized by E-Cad staining) appeared as a straight line under estrogenic conditions, Fulv treatment led to irregular, highly curved cell membranes reminiscent of bubble wrap. This Fulv-induced reorganization of AJs could also be visualized by other components of the AJ complexes including β-Catenin, α-Catenin, p120-Catenin, and the cortical actin cytoskeleton (Figure S1A). Interestingly, this effect was specifically restricted to AJs and could not be observed at the level of tight junctions as shown by ZO-1 staining (Figure 1B, xy sections). Despite this profound influence on AJ morphology, the integrity of the cellular monolayer and the polarized apicobasal localization of ZO-1 and E-Cad remained preserved (Figure 1B, xz sections). The AJ reorganization process started about 24 h after Fulv treatment and rose to full phenotype manifestation across the entire monolayer until 48 h (Figure 1C). Notably, even a shorter stimulation with Fulv for 24 h was sufficient to reorganize AJs without further Fulv treatment required (Figure 1D). This suggests that Fulv does not have an immediate effect on AJs and argues for downstream signaling events to be involved in AJ reorganization.

To test, if other anti-estrogenic compounds were able to induce AJ reorganization, we used additional anti-estrogens that interfered with ERα signaling activity through different modes of action (Figures 1E–1H', S1B, and S1C). Whereas selective estrogen receptor modulators (SERMs) such as Tamoxifen (Tam) and its hydroxylated active metabolite (4-OHT) typically perturb ERα signaling activity by competing with estrogens for receptor binding, selective estrogen receptor degraders (SERDs) like Fulv and ZK164015 additionally reduce available ERα protein levels. Importantly, all of these anti-estrogens induced the characteristic AJ phenotype (Figures 1E, 1F, S1B, and S1C) and inhibited ERα signaling activity as shown by the downregulation of the mRNA expression levels of the widely used ERα target gene *TFF1* (Figure 1G). As expected, Fulv treatment also led to a reduction of ERα protein levels as shown by immunofluorescence staining and western blotting (Figures 1E, 1H, and 1H'). Interestingly, treatment with 4-OHT, however, resulted in a rather unexpected increase of total ERα protein along with an increase in its nuclear levels, whereas no effect on its mRNA (*ESR1*) expression was detectable (Figures 1F–1H'). This was particularly surprising since inactivity of estrogen signaling is commonly associated with low nuclear ERα levels (Tecalco-Cruz et al., 2017).

We further tested for a possible role of ERβ in AJ reorganization using the potent and highly selective ERβ antagonist PHTPP (Figure S1D). However, even treatment with 1μM PHTPP did not influence the organization of AJs, which is in line with the finding that the MCF7 cell line used in this study did not express detectable protein levels of ERβ (Figure S1E). To confirm that anti-estrogen-mediated AJ reorganization was caused by the specific inhibition of the ERα signaling pathway, we depleted ERα protein levels by transfecting cells with small interfering RNAs (siRNAs) targeting *ESR1* (Figures 1I–1K'). The direct knockdown of ERα itself sufficed for the striking reorganization of AJs (Figure 1I), indicating that the effect of anti-estrogens on AJ organization was indeed mediated through inhibition of ERα signaling.
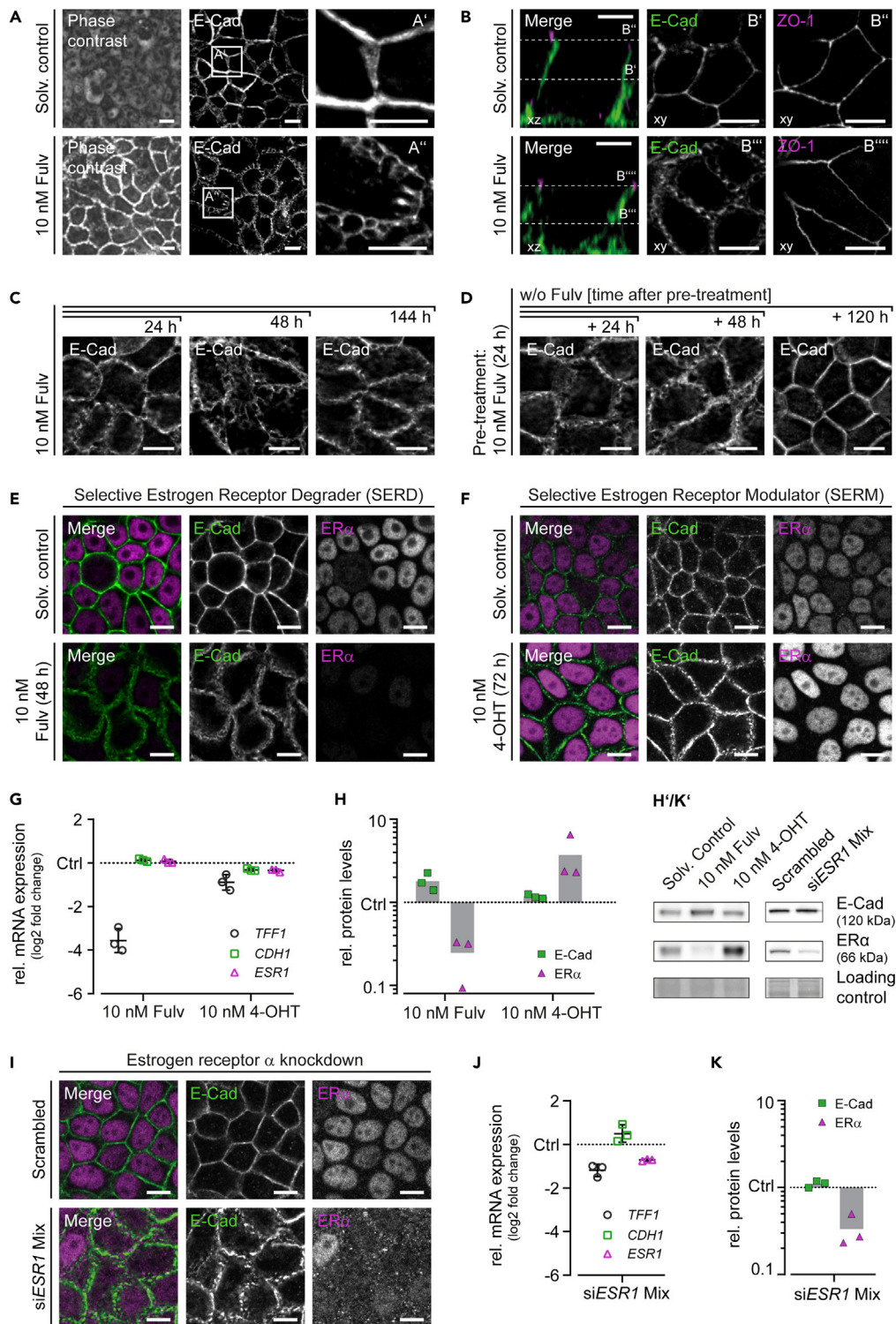
A

Solv. control — Phase contrast — E-Cad — A'

10 nM Fulv — Phase contrast — E-Cad — A''

B

Solv. control — Merge (xz) — E-Cad B' (xy) — ZO-1 B'' (xy)

10 nM Fulv — Merge (xz) — E-Cad B''' (xy) — ZO-1 B'''' (xy)

C

10 nM Fulv — 24 h — 48 h — 144 h — E-Cad

D

w/o Fulv [time after pre-treatment]

Pre-treatment: 10 nM Fulv (24 h) — + 24 h — + 48 h — + 120 h — E-Cad

E — Selective Estrogen Receptor Degrader (SERD)

Solv. control — Merge — E-Cad — ERα

10 nM Fulv (48 h) — Merge — E-Cad — ERα

F — Selective Estrogen Receptor Modulator (SERM)

Solv. control — Merge — E-Cad — ERα

10 nM 4-OHT (72 h) — Merge — E-Cad — ERα

G

rel. mRNA expression (log2 fold change)

10 nM Fulv — 10 nM 4-OHT

○ *TFF1*
□ *CDH1*
△ *ESR1*

H

rel. protein levels

10 nM Fulv — 10 nM 4-OHT

■ E-Cad
▲ ERα

H'/K'

Solv. Control — 10 nM Fulv — 10 nM 4-OHT — Scrambled — si*ESR1* Mix

E-Cad (120 kDa)
ERα (66 kDa)
Loading control

I — Estrogen receptor α knockdown

Scrambled — Merge — E-Cad — ERα

si*ESR1* Mix — Merge — E-Cad — ERα

J

rel. mRNA expression (log2 fold change)

si*ESR1* Mix

○ *TFF1*
□ *CDH1*
△ *ESR1*

K

rel. protein levels

si*ESR1* Mix

■ E-Cad
▲ ERα

Figure 1. Reorganization of Adherens Junctions (AJs) Upon Treatment with Anti-estrogens

(A) Phase contrast and immunofluorescence images showing intercellular spacing and organization of AJs upon Fulv treatment for 48 h as compared with the solvent control. White boxes indicate enlarged cell membrane areas shown in A'-A''. Scale bars, 10 μm.

Figure 1. *Continued*

(B) Optical sections from immunofluorescence images showing organization of tight junctions (ZO-1, magenta) and AJs (E-Cad, green) upon Fulv treatment for 48 h as compared with the solvent control. White dashed lines in xz sections indicate image planes of xy sections shown in B′-B″″′. Scale bars, 10 μm.

(C) Immunofluorescence images showing AJ organization (E-Cad) upon Fulv treatment for 24, 48, and 144 h. Scale bar, 10 μm.

(D) Immunofluorescence images showing AJ organization (E-Cad) upon short-term pre-treatment with Fulv for 24 h. Indicated time points depict time after removal of Fulv-containing medium. Scale bar, 10 μm.

(E and F) Immunofluorescence images showing AJ organization (E-Cad, green) and ERα protein levels (magenta) upon treatment with the selective estrogen receptor degrader (SERD) Fulv for 48 h and treatment with the selective estrogen receptor modulator (SERM) 4-hydroxytamoxifen (4-OHT) for 72 h as compared with the solvent control. Scale bar, 10 μm.

(G) Quantitative RT-PCR measurement of ERα (*ESR1*, magenta) and E-Cad (*CDH1*, green) mRNA expression levels upon treatment with Fulv and 4-hydroxytamoxifen (4-OHT) for 48 h. The mRNA expression levels of the ERα target gene *TFF1* serve as readout for ERα signaling activity. Relative mRNA expression levels are normalized to the solvent control (Ctrl). Biological replicates, n = 3. Error bars, mean $\pm$ SD.

(H) Western blot analysis and quantification of ERα (magenta) and E-Cad (green) protein levels upon treatment with Fulv and 4-hydroxytamoxifen (4-OHT) for 48 h. Relative protein expression levels are normalized to the solvent control (Ctrl). Biological replicates, n = 3. Bars, mean of biological replicates.

(H′) Representative western blots of quantification shown in (H). Loading control, Coomassie total protein staining.

(I) Immunofluorescence images showing AJ organization (E-Cad, green) and ERα protein levels (magenta) of cells transfected with a pool of four different *ESR1* siRNAs compared with cells transfected with scrambled control siRNA for 72 h. Scale bar, 10 μm.

(J) Quantitative RT-PCR measurement of ERα (*ESR1*, magenta) and E-Cad (*CDH1*, green) mRNA expression levels upon transfection of cells with a mix of four different *ESR1* siRNAs for 72 h. The mRNA expression levels of the ERα target gene *TFF1* serve as readout for ERα signaling activity. Relative mRNA expression levels are normalized to the scrambled control (Ctrl). Biological replicates, n = 3. Error bars, mean $\pm$ SD.

(K) Western blot analysis and quantification of ERα (magenta) and E-Cad (green) protein levels upon transfection of cells with a mix of four different *ESR1* siRNAs for 72 h. Relative protein expression levels are normalized to the scrambled control (Ctrl). Biological replicates, n = 3. Bars, mean of biological replicates.

(K′) Representative western blots of quantification shown in (K). Loading control, Coomassie total protein staining.

See also Figure S1.

Quantification of Estrogen-Dependent Adherens Junction Reorganization

In order to quantify the estrogen-dependent morphology of AJs throughout the cellular monolayer and across multiple experimental conditions, we built a CellProfiler/CellProfiler Analyst (CP/CPA)-based quantitative image analysis pipeline that classified cells into the two categories "continuous AJs" and "discontinuous AJs" (see Transparent Methods section for further details) (Figure 2A). This image analysis pipeline included two main steps, i.e., (1) the E-Cad staining-based automatic detection of cell membranes (segmentation) and extraction of morphological parameters and (2) the subsequent parameter-based binary classification of individual cells by supervised machine learning (classification). This way, the organization of AJs of all cells in each individual image was scored and represented as a number, termed Morphology Index (MI), that depicts the fraction of cells showing continuous AJs (quantification) (Figure 2A′). For example, the Fulv-induced switch from continuous to discontinuous AJs is reflected by a decrease of the MI. Note that, in all of the following quantifications, the MI (fraction of cells showing continuous AJs) was normalized to a range from 0 to 1, with 1 indicating the solvent (negative) control and 0 indicating the 10 nM Fulv (positive) control.

We applied this CP/CPA pipeline to analyze the organization of AJs upon treatment of cells with increasing concentrations of Fulv (anti-estrogenic conditions) and upon treatment with a fixed dose of 10 nM Fulv in combination with increasing concentrations of the endogenous estrogen 17β-Estradiol (E2) (estrogenic conditions) (Figure 2B). In this ERα signaling modulation experiment, Fulv treatment induced the reorganization of AJs in a dose-dependent manner (Figure 2B, left), which could be rescued by co-treatment with E2 (Figure 2B, right). Notably, a dose of 1–10 nM Fulv and 0.1–1 nM E2 appeared to be saturating under these anti-estrogenic and estrogenic conditions, which correlated with the published ERα-binding affinities of the two compounds in a competitive situation (Wakeling et al., 1991). We finally used the CP/CPA pipeline to analyze the organization of AJs upon ERα knockdown shown in Figure 1I. Again, the ERα-dependent reorganization of AJs could be detected throughout the cellular monolayer upon transfection of cells with four different *ESR1* siRNAs individually (#4–#11) and in combination (Mix).

This quantitative image analysis approach further facilitated the time-resolved analysis of the kinetics of the AJ reorganization process in living cells by live-cell fluorescence microscopy. Using another MCF-7 cell line
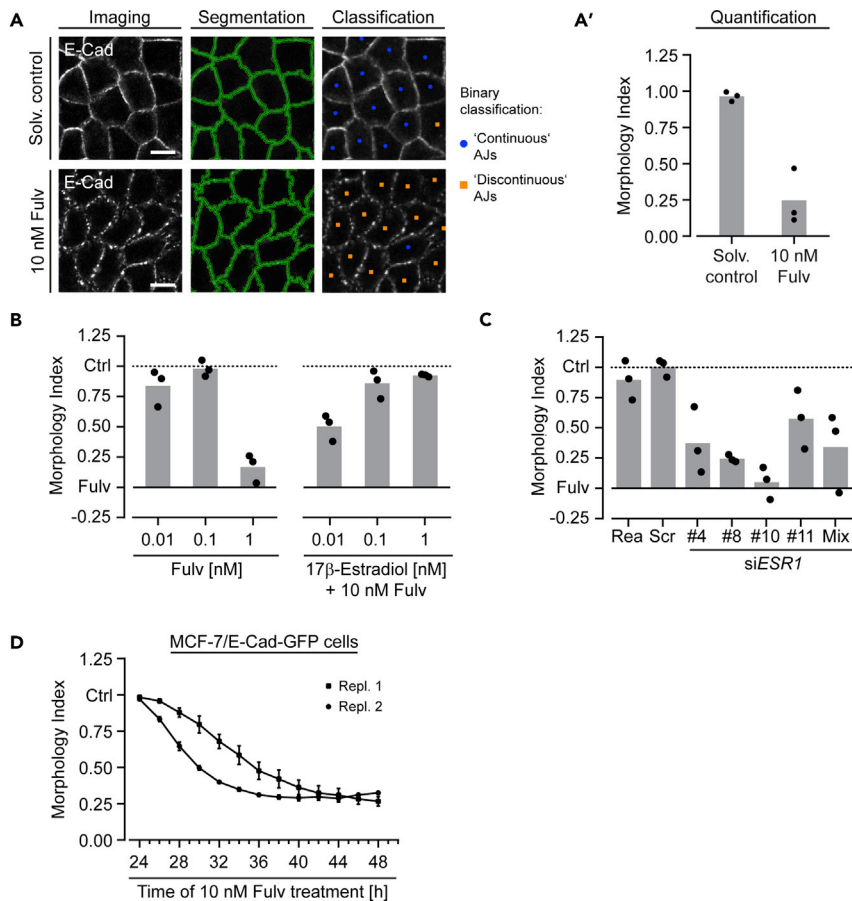
Figure 2. Quantification of Adherens Junction (AJ) Reorganization

(A) Main steps of a CellProfiler/CellProfiler Analyst (CP/CPA)-based image analysis pipeline including segmentation and classification of immunofluorescence images (E-Cad staining) to categorize cells into "Continuous AJs" (blue circles) and "Discontinuous AJs" (orange squares) based on their AJ organization.

(A′) Representative results of a CP/CPA-based analysis of the AJ organization in cells treated with Fulv for 48 h or solvent control-treated cells. The plot shows the fraction of cells classified as Continuous AJs (Morphology Index, MI) for each condition. The reorganization of AJs upon Fulv treatment results in an increase of Discontinuous AJs and therefore a decrease of the MI. Each data point represents an average MI from three individual images per treatment condition. Biological replicates, n = 3. Bars, mean of biological replicates.

(B) Application of the CP/CPA-based image analysis pipeline on images from ERα signaling inhibition (Fulv titration) and restoration (10 nM Fulv in combination with 17β-Estradiol titration) experiments. The derived MI is normalized to the negative control (solvent, Ctrl = 1) and the positive control (10 nM Fulv, Fulv = 0). Each data point represents an average MI from three individual images per treatment condition. Biological replicates, n = 3. Bars, mean of biological replicates.

(C) Quantification of AJ organization upon transfection with four different *ESR1* siRNAs individually and in combination (Mix) compared with controls with scrambled siRNA (Scr) or transfection reagent only (Rea). The MI is normalized to the negative control (solvent, Ctrl = 1) and positive control (10 nM Fulv, Fulv = 0). Biological replicates, n = 3. Bars, mean of biological replicates.

(D) Time-resolved quantification of AJ reorganization in MCF-7/E-Cad-GFP cells (stably expressing an *E-Cad::GFP* plasmid) upon Fulv treatment. Cells were imaged every 2 h by live-cell fluorescence microscopy over the course of 24 h after pre-treatment with Fulv for 24 h. Image analysis was performed using the commercial Harmony software (PerkinElmer) following the principle as described in (A). Biological replicates, n = 2. Error bars, mean ± SD of three technical replicates.

See also Videos S1 and S2.

that constitutively expressed GFP-tagged E-Cad (de Beco et al., 2009) (Figure 2D; Videos S1 and S2), we monitored and quantified the reorganization of AJs under anti-estrogenic conditions over the course of 24 h. Although no reorganization of AJs could be observed in MCF-7/E-Cad-GFP cells during the first 0–24 h upon Fulv treatment as compared with the solvent control (MI = 1), the MI gradually decreased
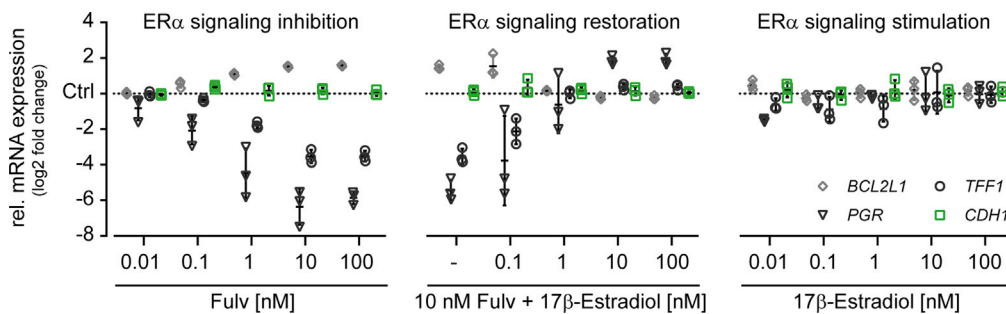
Figure 3. ERα Signaling Activity under Anti-estrogenic and Estrogenic Conditions

Quantitative RT-PCR measurement of mRNA expression levels of typical ERα target genes (*BCL2L1*; *PGR*; *TFF1*) and E-Cad (*CDH1*, green) upon ERα signaling inhibition (Fulv titration), restoration (10 nM Fulv in combination with 17β-Estradiol titration), and stimulation (17β-Estradiol titration) for 48 h. Relative mRNA expression levels for each treatment condition are normalized to the respective solvent control (Ctrl). Biological replicates, n = 3. Error bars, mean ± SD.

between 24 and 48 h. This time-resolved analysis revealed that (1) the organization of AJs was sensitive to Fulv treatment also in MCF-7/E-Cad-GFP cells and (2) the AJ reorganization process occurred within a very similar time frame as compared with the MCF-7 cell line with only endogenous E-Cad expression (see Figure 1C).

Physiological E2 Levels Impact Spatial Adherens Junction Organization

To further substantiate that the organization of AJs correlated with the activity of the ERα signaling pathway, we analyzed the gene expression levels of the widely used ERα target genes *BCL2L1*, *PGR*, and *TFF1* under anti-estrogenic and estrogenic conditions (Figure 3) as described in the ERα signaling modulation experiment (see Figure 2B). As expected, Fulv treatment stimulated *BCL2L1* expression and efficiently inhibited the transcription of *PGR* and *TFF1* in a dose-dependent manner (Figure 3, left). In turn, application of a fixed dose of 10 nM Fulv in combination with increasing concentrations of E2 restored ERα target gene expression levels in a dose-dependent manner (Figure 3, middle). Notably, the expression levels of *PGR* were even hyper-stimulated under co-treatment conditions at higher E2 concentrations. In contrast, a stimulation with E2 alone did not change expression levels of these ERα target genes indicating that ERα activity was already saturated (Figure 3, right), even though all experiments were performed in reduced-serum medium using fetal calf serum (FCS) with particularly low hormone levels. This was, however, expected to some extent since the parental MCF-7 cell line was particularly selected for high estrogen sensitivity and reported to respond to very low E2 concentrations reaching a plateau already at 10 pM (Villalobos et al., 1995). In this study, the cell culture medium still contained a final E2 concentration of 3.4–4.1 pM, which is in the range of physiological E2 levels in postmenopausal women (Rothman et al., 2011). An additional stimulation of cells with E2 alone was most likely not possible since the co-factors involved in the downstream regulation of ERα-mediated gene expression are rate limiting (List et al., 2001). However, when Fulv was present under co-treatment conditions, the total levels of available ERα were efficiently depleted (see Figures 1E, 1H and 1H'), which presumably led to a reduced sequestration of the involved co-factors and a hyper-stimulation of E2-responsive gene expression.

This ERα signaling modulation experiment further revealed that a dose of 10 nM Fulv and 1 nM E2 appeared to be saturating with regard to the regulation of ERα target gene expression levels under anti-estrogenic and estrogenic conditions, which correspond to the concentrations at which AJ reorganization was induced or rescued (see Figure 2B). Hence, these data suggest that physiologically relevant E2 levels influence the organization of AJs and estrogen signaling activity in breast cancer cells.

Spatial Adherens Junction Reorganization Leads to Microclusters of E-Cad in the Cell Membrane

It has previously been reported that estrogen signaling regulates gene expression levels of E-Cad in multiple breast cancer cell lines, but partially contradicting models (stimulation versus inhibition of *CDH1* expression) have been proposed (Cardamone et al., 2009; Fujita et al., 2003; Oesterreich et al., 2003; Ye et al., 2008, 2010). Interestingly, in the present study, inhibition, or restoration, or stimulation of ERα signaling did not clearly alter E-Cad transcription levels in the MCF-7 cell line that we used (Figures 1G, 1J, and 3, green). In fact, E-Cad protein was always detectable by immunofluorescence staining (Figures
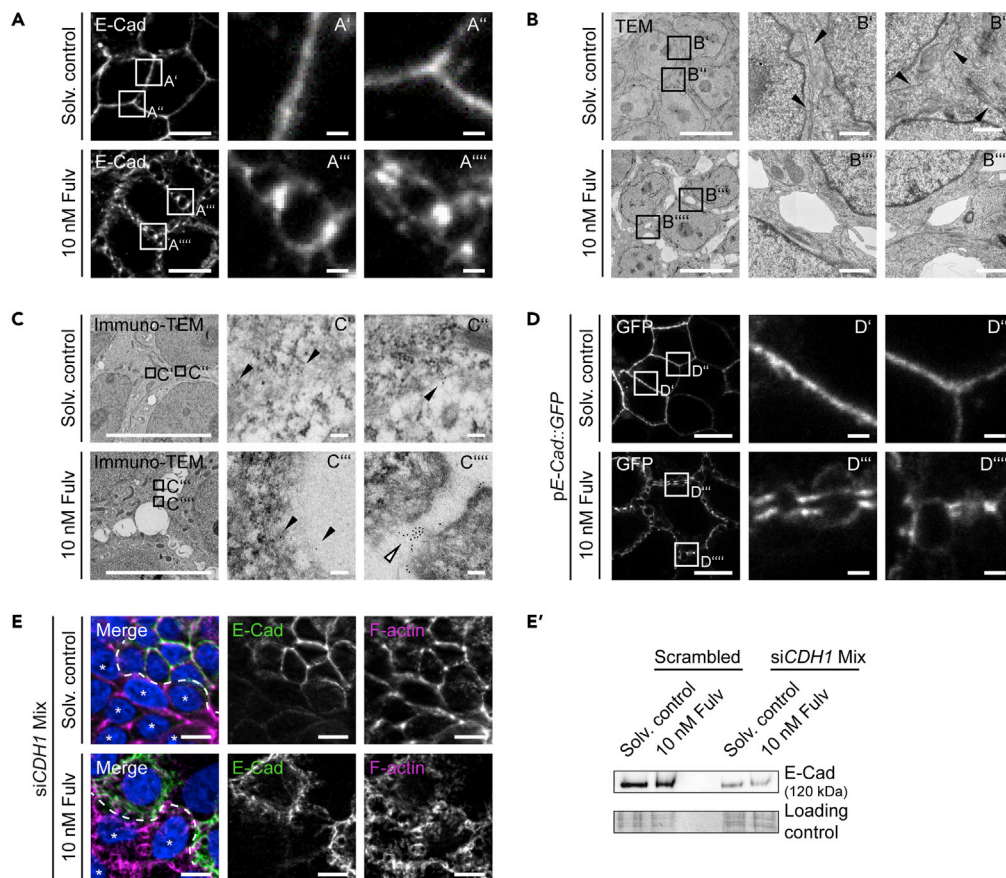
Figure 4. Clustering of E-Cad at Cell Membranes under Anti-estrogenic Conditions

(A) High-resolution immunofluorescence images showing AJ organization (E-Cad) and formation of E-Cad microclusters upon Fulv treatment for 48 h as compared with the solvent control. White boxes indicate enlarged cell membrane areas shown in A′-A″″. Scale bars, 10 and 1 μm.

(B) Transmission electron microscopy (TEM) images showing the organization of cell-cell contact zones upon Fulv treatment for 48 h as compared with the solvent control. Black boxes indicate enlarged cell membrane areas shown in B′-B″″. Arrowheads indicate cell membranes. Scale bars, 10 and 1 μm.

(C) Transmission electron microscopy images showing localization of immuno-gold-labeled E-Cad molecules (Immuno-TEM) upon Fulv treatment for 48 h as compared with the solvent control. Black boxes indicate enlarged cell membrane areas shown in C′-C″″. Black arrowheads indicate individual gold particles along cell membranes. White arrowheads indicate gold particle clusters along remaining cell-cell contact zones. Scale bars, 1 and 0.1 μm.

(D) Fluorescence images showing AJ organization (GFP) and formation of E-Cad microclusters in Fulv-treated cells expressing an *E-Cad::GFP* plasmid (p*E-Cad::GFP*) for 48 h as compared with the solvent control. Transfected cells are visualized by GFP expression. White boxes indicate enlarged cell membrane areas shown in D′-D″″. Scale bars, 10 and 1 μm.

(E) Immunofluorescence images showing Fulv-treated and solvent control-treated cells upon siRNA-mediated E-Cad (*CDH1*) knockdown for 48 h. Cells transfected with a pool of four different siRNAs (si*CDH1*) show reduced E-Cad protein levels (green). F-Actin staining (magenta) visualizes the cortical F-Actin network and serves as a proxy for AJ organization in knockdown cells (asterisks). Scale bar, 10 μm.

(E′) Representative western blot of experiment shown in (E). Loading control, Coomassie total protein staining.
See also Figure S2.

1A–1F, 1I, 2B, 2C, S1B, and S1C) and western blotting (Figures 1H, 1H′, 1K, and 1K′) under anti-estrogenic and estrogenic conditions.

However, as part of the AJ reorganization process, we also observed the emergence of prominent micrometer-scale E-Cad clusters at cell membranes upon Fulv treatment (Figure 4A). To better resolve the distribution of E-Cad in the cell membrane, we performed transmission electron microscopy (TEM) of Fulv-treated and control cells. Conventional TEM showed that the direct cell-cell contact area was significantly reduced in Fulv-treated

Patient ID[a]	Data from This Study		Metadata from METAcancer Project								
	E-Cad Status	ERa Localization	Tumor Morphology	Grading	T Stage	N Stage	ER Score	ER Percent[b]	PR Score	PR Percent[b]
META-83	Positive	Cytoplasmic	IDC, invasive carcinoma of no special type	3	1	1	0	NA	0	NA
META-321	Unclear	Cytoplasmic	IDC, invasive carcinoma of no special type	3	2	2	0	NA	0	NA
META-292	Positive	Cytoplasmic	IDC, invasive carcinoma of no special type	1	1	1	0	NA	0	NA
META-357	Positive	Nuclear	IDC, invasive carcinoma of no special type	2	1	2	1	80	0	NA
META-100	Positive	Nuclear	IDC, invasive carcinoma of no special type	3	2	1	1	81	0	NA
META-365	Positive	Nuclear	IDC, invasive carcinoma of no special type	2	1	0	1	90	1	60
META-23	Positive	Nuclear	IDC, invasive carcinoma of no special type	2	1	0	1	NA	0	NA
META-327	Positive	Cytoplasmic	IDC, invasive carcinoma of no special type	2	2	0	1	20	0	NA
META-228	Positive	Both	IDC, invasive carcinoma of no special type	3	2	0	0	NA	0	NA
META-222	Positive	Nuclear	IDC, invasive carcinoma of no special type	2	1	3	1	100	1	70
META-450	Positive	Nuclear	IDC, invasive carcinoma of no special type	3	3	0	1	NA	0	NA
META-102	Positive	Cytoplasmic	IDC, invasive carcinoma of no special type	2	4	0	1	100	0	0
META-240	Positive	Both	IDC, invasive carcinoma of no special type	3	1	0	1	80	1	20
META-204	positive	Both	IDC, invasive carcinoma of no special type	3	2	1	1	60	1	70
META-280	Positive	Cytoplasmic	IDC, invasive carcinoma of no special type	2	2	0	0	0	0	NA
META-277	Positive	Nuclear	IDC, invasive carcinoma of no special type	2	1	0	1	80	1	40

Table 1. Analysis of Breast Tumor Tissue Samples from METAcancer Project

E-Cad expression status and predominant ERα localization in breast tumor tissue samples from patients with diagnosed invasive ductal carcinoma (IDC). Samples obtained from METAcancer project (representative immunofluorescence images shown in Figures 5 and S2).

NA, no data available. See also Figures S1 and S2.

[a]Numbers of histological sections were anonymized.

[b]ER/PR percent = fraction of nuclear staining observed for ERα (ER) and progesterone receptor (PR) in diagnostic sections.

cells (Figure 4B). Furthermore, Immuno-TEM using immuno-gold labeling of E-Cad revealed that E-Cad protein density was increased at the remaining cell-cell contacts (Figure 4C, arrowheads), indicating the formation of locally restricted focal clusters of E-Cad consistent with observations by immunofluorescence microscopy.

To analyze the influence of E-Cad protein levels for AJ reorganization, we modulated its expression levels by either overexpression of E-Cad using a plasmid encoding *E-Cad::GFP* (Figure 4D) or depletion of E-Cad
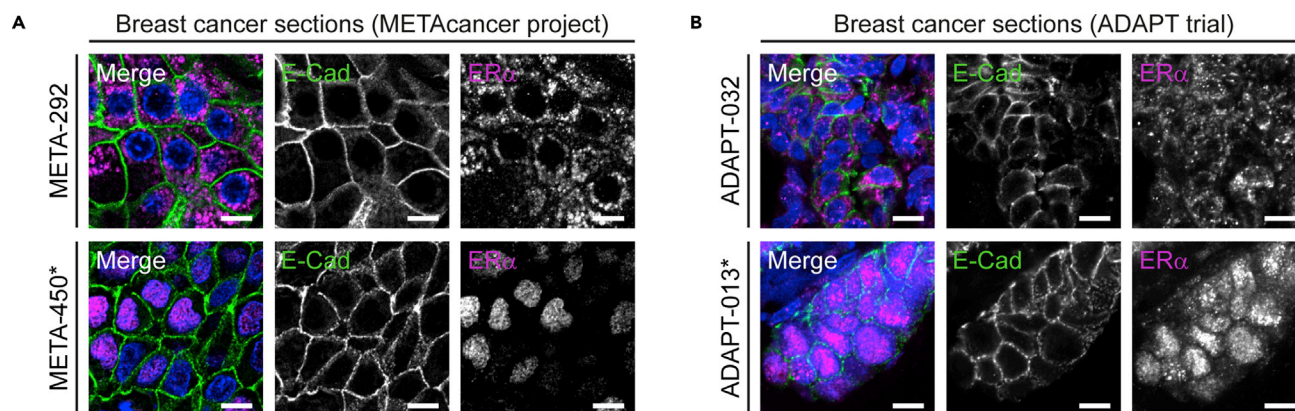
Figure 5. Analysis of Breast Tumor Tissue Samples from METAcancer Project and ADAPT Trial

(A and B) Immunofluorescence images showing AJ organization (E-Cad, green) and ERα localization (magenta) in representative breast tumor tissue samples from patients with diagnosed invasive ductal carcinoma (IDC). An asterisk indicates sections with clustered appearance of E-Cad along cell membranes. Samples obtained from (A) METAcancer project and (B) ADAPT trial (results summarized in Table 1 and Table 2). The numbers of histological sections were anonymized. Scale bar, 10 μm.

See also Figures S1 and S2.

using siRNA targeting *CDH1* (Figures 4E, 4E′, and S2B). As shown in Figure 4D, the increase of cellular E-Cad protein levels by p*E-Cad::GFP* overexpression was not sufficient to induce AJ reorganization in solvent control-treated cells. In line with the data shown for the MCF-7/E-Cad-GFP cell line (see Figure 2D), Fulv treatment also led to the formation of E-Cad microclusters in cells that only transiently expressed p*E-Cad::GFP*. Furthermore, the efficient reduction of E-Cad levels by siRNA knockdown did also not influence the Fulv-induced reorganization of AJs as shown by actin immunostaining (Figure 4E, asterisks; Figure S2B). Even though E-Cad certainly remains functionally required for the general maintenance of cell-cell contacts even under knockdown conditions, these data suggest that changes in total E-Cad protein levels apparently do not influence the anti-estrogen-mediated reorganization of AJs per se. The observed changes in the local distribution of E-Cad at the cell membrane under anti-estrogenic and estrogenic conditions rather implicate an estrogen-dependent modulation of E-Cad protein membrane turnover, processing or trafficking instead of an estrogen-dependent transcriptional regulation of E-Cad expression.

Spatial Organization of Adherens Junctions and Microclustering of E-Cad Observed in Breast Tumor Tissue Samples

In order to evaluate how the estrogen-dependent organization of AJs in breast cancer cells translates into a clinical setting, we tested whether comparable effects could also be observed *in vivo*. We first analyzed breast tumor tissue samples of patients with diagnosed IDC that were collected by the METAcancer consortium (Denkert et al., 2012). As expected for IDC, ERα and E-Cad were both detectable in most samples (15/16 patients) (Table 1; Figures 5A and S2A). However, the localization of ERα (ranging from predominantly nuclear to cytoplasmic) and particularly the morphology of cell-cell contacts (ranging from uniform to more clustered E-Cad distribution) considerably varied between patients.

In addition, we more specifically analyzed the effects of anti-estrogen treatment on estrogen signaling in breast cancer using breast tumor tissue samples of patients with histologically confirmed primary invasive breast carcinoma who underwent neoadjuvant endocrine therapy in the context of the ADAPT clinical trial (Hofmann et al., 2013). For this analysis, the number of available patient material was, however, limited to post-neoadjuvant samples from three patients who fulfilled the required criteria for the hormone receptor (HR) and HER2 expression status (HR+/HER2-), as well as for the corresponding subtype-specific treatment regime of the induction therapy (daily 20 mg Tamoxifen for 3–4 weeks) to allow comparison with the *in vitro* data (Table 2; Figures 5B and S1F). Among these samples, the distribution of E-Cad along the cell membrane again varied between patients in a similar way as observed in the METAcancer cohort. Surprisingly, despite Tam treatment for at least 21 days, a predominantly nuclear ERα localization could still be observed in two of three samples. Considering that we observed a similar effect of 4-OHT on nuclear ERα levels *in vitro* (see Figure 1F), these data together suggest that nuclear ERα localization *per se* is not necessarily a sufficient biomarker to assess estrogen signaling activity *in vitro* and *in vivo*. Moreover, the observed differences in the distribution of E-Cad ranging from uniform

Patient ID[a]	Data from This Study		Metadata from ADAPT Trial									
	E-Cad Status	ERa Localization	Tumor Morphology	Treatment	Age	Grading	T Stage	N stage	ER Score	ER Percent[b]	PR Score	PR Percent[b]
ADAPT-009	Positive	Cytoplasmic	IDC, invasive carcinoma of no special type	21 d Tamoxifen	61	2	2	0	1	80 (100)	1	80 (80)
ADAPT-032	Positive	Both	IDC, invasive carcinoma of no special type	21–28 d Tamoxifen	68	3	1c	0	1	NA (100)	1	NA (50)
ADAPT-013	Positive	Nuclear	IDC, invasive carcinoma of no special type	21 d Tamoxifen	46	2	1c	0	1	100 (90)	1	100 (100)

Table 2. Analysis of Breast Tumor Tissue Samples from ADAPT Trial

E-Cad expression status and predominant ERα localization in breast tumor tissue samples from patients with diagnosed invasive ductal carcinoma (IDC). Samples obtained from ADAPT trial (representative immunofluorescence images shown in Figures 5 and S1).

NA, no data available. See also Figures S1 and S2.

[a]Numbers of histological sections were anonymized.

[b]ER/PR percent = fraction of nuclear staining observed for ERα (ER) and progesterone receptor (PR) in diagnostic sections before and after (in brackets) Tam treatment.

to clustered was to some extent comparable between the *in vitro* and *in vivo* data. Hence, these data provide a starting point for future studies investigating a potential clinical relevance of estrogen-dependent AJ organization for breast cancer progression and metastasis.

Functional Consequences of Estrogen-Dependent Adherens Junction Reorganization

Actomyosin-Dependent Adherens Junction Reorganization Increased Cell Stiffness of Breast Cancer Cells

The organization of AJs and the distribution of E-Cad along cell membranes is a dynamically regulated multi-step process that depends on calcium-dependent homophilic E-Cad binding and on the activity of the actomyosin network (Nelson, 2008). To address the role of the actomyosin network for Fulv-induced AJ reorganization, we interfered with actomyosin network dynamics by (1) inhibiting actin filament polymerization using Latrunculin A (LatA) (Figures 6A and S3A) and (2) reducing Myosin-II motor protein activity using the ROCK inhibitor Y-27632 (Figures 6B and S3B). In both cases, pre-treatment of cells with Fulv for 48 h induced the characteristic AJ phenotype, which could be considerably reverted by the short-term application of LatA for 30 min or Y-27632 for 10 h (Figures 6A, 6B, S3A, and S3B, +0 h). Notably, the AJ phenotype reformed within 14 h after switching back to Fulv only containing medium indicating that actomyosin network activity was restored again (Figures 6A, 6B, S3A, and S3B, +14 h). These data support a direct role of the actomyosin network in anti-estrogen-mediated AJ reorganization.

Since the activity of the actomyosin network also determines the biomechanical properties including stiffness of cells (Omidvar et al., 2014), we performed atomic force microscopy (AFM) indentation measurements on confluent cell monolayers (Figures 6C and 6D). The stiffness of Fulv-treated cells was generally elevated compared with solvent control-treated cells (Figure 6C), which applied to both the cell surface area and junctional regions (Figure 6D) suggesting that the actomyosin network was more constricted under anti-estrogenic conditions. To investigate potential matrix-dependent influences of anti-estrogen-mediated AJ reorganization, we grew cells on different extracellular matrix constituents including fibronectin and laminin (Figure 6E). However, none of these surface coatings influenced the reorganization of AJ upon Fulv treatment. Together, these results show that estrogen signaling influences actomyosin network activity and the biomechanical properties of breast cancer cells, thereby regulating the organization of AJs.

Spatial Reorganization of Adherens Junctions Increased Stability of Cell-Cell Contacts and Decreased Cell Motility

Since estrogen signaling inhibition led to a strong reduction of the cell-cell contact area and formation of E-Cad microclusters (see Figures 5A–5C), we next analyzed the effect of anti-estrogen treatment on AJ
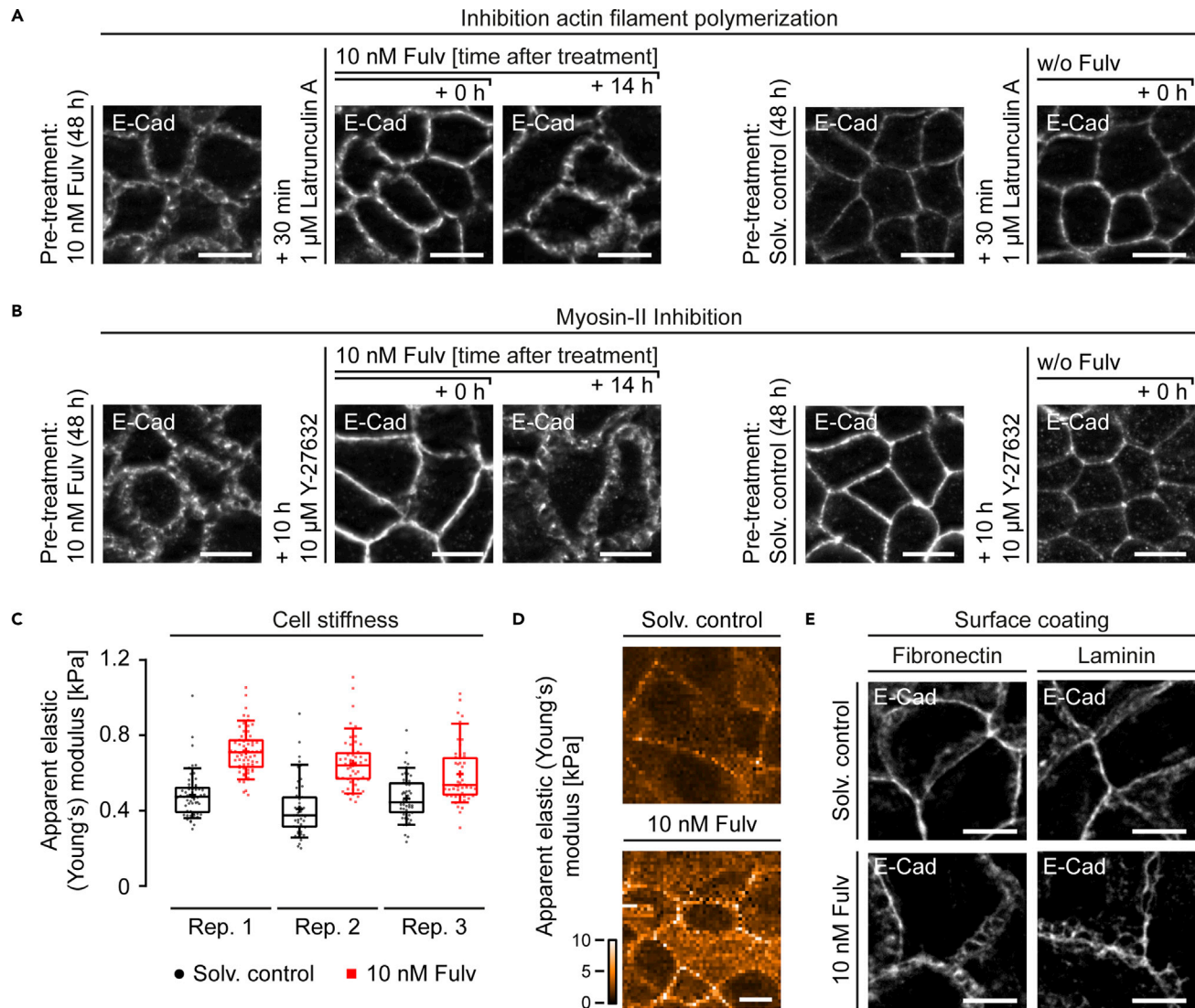
Figure 6. Role of the Actomyosin Cytoskeleton for Adherens Junction Reorganization and Biomechanical Properties of Cells

(A) Immunofluorescence images showing AJ organization (E-Cad) in Fulv-treated cells and solvent control-treated cells after pre-treatment for 48 h and after application of Latrunculin A-containing medium (1 μM Latrunculin A for 30 min) to depolymerize the actin cytoskeleton. Indicated time points depict time after removal of Latrunculin A-containing medium. Scale bar, 10 μm.

(B) Immunofluorescence images showing AJ organization (E-Cad) in Fulv-treated cells and solvent control-treated cells after pre-treatment for 48 h and after application of Rho-associated, coiled-coil containing protein kinase (ROCK) inhibitor-containing medium (10 μM Y-27632 for 10 h) to reduce the Myosin-II motor protein activity. Indicated time points depict time after removal of Y-27632-containing medium. Scale bar, 10 μm.

(C) Quantification of cell stiffness (Apparent elastic [Young's] modulus) by atomic force microscopy (AFM) indentation measurements on cells treated with Fulv for 48 h (red datasets, $E_{Repl.1} = 0.71 \pm 0.12$ kPa; $E_{Repl.2} = 0.65 \pm 0.14$ kPa; $E_{Repl.3} = 0.59 \pm 0.16$ kPa; mean $\pm$ SD) as compared with solvent control-treated cells (black datasets, $E_{Repl.1} = 0.48 \pm 0.12$ kPa; $E_{Repl.2} = 0.41 \pm 0.15$ kPa; $E_{Repl.3} = 0.47 \pm 0.12$ kPa). Biological replicates, n = 3. Boxes, 25th, 50th (median), and 75th percentiles. Whiskers, 10th and 90th percentiles. Cross, mean for each group.

(D) Apparent elastic (Young's) modulus distribution maps of 50 × 50 μm regions of cells treated with Fulv for 48 h as compared with solvent control-treated cells at a spatial resolution of 1 μm. Scale bar, 10 μm.

(E) Immunofluorescence images showing AJ organization (E-Cad) of cells grown on extracellular matrix constituents (fibronectin, laminin) upon Fulv treatment for 48 h as compared with the solvent control. Scale bar, 10 μm.

See also Figure S3.

stability and cell motility. In order to assess the fraction of E-Cad molecules that engage in cell-cell contact formation, we studied the resilience of E-Cad to extracellular cleavage by trypsin (trypsin assay). Short-term treatment of solvent control-treated cells with trypsin resulted in a decrease of full-length E-Cad (120 kDa)
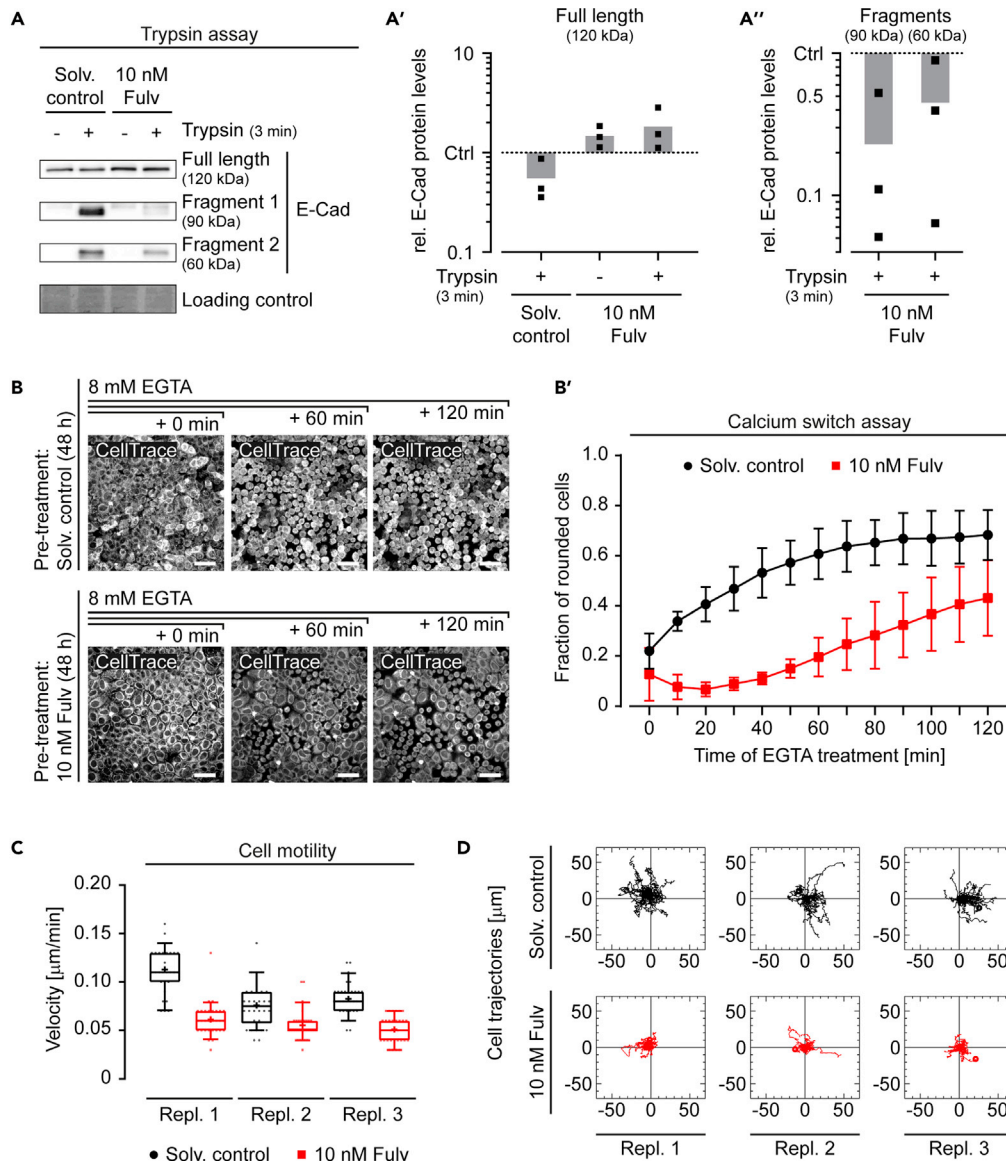
Figure 7. Adherens Junction (AJ) Stability and Cell Motility under Anti-estrogenic Conditions

(A) Representative western blots showing full-length E-Cad (120 kDa) protein and E-Cad fragment (90 kDa, 69 kDa) bands upon application of trypsin-containing medium for 3 min to disrupt AJs. Loading control, Coomassie total protein staining.

(A') Western blot analysis and quantification of full-length E-Cad protein levels of experiment shown in (A) normalized to solvent control (without trypsin treatment, Ctrl). Biological replicates, n = 3. Bars, mean of biological replicates.

(A'') Western blot analysis and quantification of E-Cad fragment levels of experiment shown in (A) normalized to solvent control (trypsin-treated, Ctrl). Biological replicates, n = 3. Bars, mean of biological replicates.

(B and B') Representative fluorescence images from live cell imaging (CellTrace) of cells pre-treated with Fulv for 48 h and solvent control-treated cells. Indicated time points depict time after application of EGTA-containing medium (8 mM EGTA) to disrupt AJs. The plot shown in B' displays the fraction of Fulv-treated (red dataset) and solvent control (black dataset) cells classified as "Rounded cells" over the course of 120 min. Three individual images were analyzed per time point and treatment condition using CellProfiler/CellProfiler Analyst. Biological replicates, n = 3. Error bars, mean of biological replicates +/− SD. Scale bar, 10 μm.

(C) Quantification of cell motility (velocity) by manual tracking of cells treated with Fulv for 48 h (red datasets, $V_{Repl.1}$ = 0.0613 ± 0.0176 μm/min; $V_{Repl.2}$ = 0.0553 ± 0.0157 μm/min; $V_{Repl.3}$ = 0.051 ± 0.014 μm/min; mean ± SD) as compared with solvent control-treated cells (black datasets, $V_{Repl.1}$ = 0.113 ± 0.0237 μm/min; $V_{Repl.2}$ = 0.0757 ± 0.023 μm/min; $V_{Repl.3}$ = 0.0827 ± 0.0174 μm/min). For each treatment condition, a total of 30 cells from three individual areas (10 cells per

Figure 7. *Continued*

area) were tracked every 10 min over the course of 16 h using Fiji plugins. Boxes, 25th, 50th (median), and 75th percentiles. Whiskers, 10th and 90th percentiles. Cross, mean for each group.

(D) Cell path maps comprising trajectories of individual cells tracked in Figure 7C.

See also Videos S3 and S4.

in western blot analysis and the detection of two additional E-Cad bands at around 90 kDa and 60 kDa (Figures 7A and 7A'). Interestingly, these fragment bands were strikingly less prominent upon Fulv-mediated AJ reorganization (Figures 7A and 7A''), arguing for a reduced susceptibility of E-Cad for trypsin digestion and therefore an increased participation in cell-cell contact formation.

We then tested whether the reduced susceptibility of Fulv-treated cells to trypsin digestion eventually also influenced the stability of cell-cell contacts. To analyze the stability of homophilic E-Cad binding, we treated cells with the calcium-chelating agent EGTA (calcium switch assay). Application of EGTA to both solvent control-treated cells and cells pre-treated with Fulv for 48 h led to a release of E-Cad-mediated cell-cell contacts and cell rounding over the course of 120 min, whereas the attachment to the substrate remained preserved (Figure 7B). Interestingly, the quantification of the fraction of rounded cells revealed that cells pre-treated with Fulv clearly showed a reduced rate of cell rounding (Figure 7B') suggesting that either the focal AJs themselves or the altered activity of the actomyosin network confer more stability to the cells and cell-cell contacts. These data further suggest that the observed micron-scaled E-Cad assemblies (see Figure 5) compensate for the reduced cell-cell contact area upon AJ reorganization by an increased AJ stability.

To assess other functional consequences of this increased AJ stability for the plasticity of entire cellular monolayer, we recorded the motility of confluent cells over the course of 16 h after introducing a scratch nearby the imaged region (Figures 7C and 7D; Videos S3 and S4). Notably, both the velocity of cells (Figure 7C) and the length of their trajectories (Figure 7D) were considerably reduced upon Fulv treatment indicating that the rigidity of the cellular monolayer was increased. Together, the influence of anti-estrogens on AJ stability and cell motility suggest a role of estrogen signaling in the regulation of the biomechanical properties of breast cancer cells and may also provide an explanation for the metastasis-protective effect of anti-estrogens in endocrine therapy.

ERα Regulates Reorganization of Adherens Junctions and Microclustering of E-Cad through Amphiregulin

In addition to ERα, mammary gland development is also essentially regulated through the Epidermal growth factor receptor (EGFR) and its ligand Amphiregulin (AREG), which appears to be a critical downstream effector of estrogen signaling in ERα-positive human breast tumors (McBryan et al., 2008). To verify that *AREG* is a target gene of ERα in the MCF-7 cell line used in this study, we monitored its expression levels at different time points upon Fulv treatment (Figure 8A) and further modulated ERα signaling activity as described above (Figure 8B; see Figure 2B). Indeed, *AREG* expression levels quickly decreased within a few hours upon Fulv treatment (Figure 8A) and showed a clear dose-response relationship with estrogen signaling inhibition and restoration (Figure 8B). Notably, *AREG* expression levels were hyper-stimulated under co-treatment conditions at higher E2 concentrations, which is in line with the data shown for *PGR* (see Figure 3, middle). The ERα-dependent expression of AREG could finally be confirmed by *ESR1* knockdown (Figure 8D).

Moreover, we tested whether AREG was directly involved in the anti-estrogen-mediated reorganization of AJs (Figures 8C–8G). Indeed, depletion of AREG itself was sufficient to induce the reorganization of AJs (Figures 8C and 8C'), even though its mRNA and protein levels were less efficiently reduced as compared with Fulv treatment (Figures 8B, 8D, and 8E). Importantly, the Fulv-mediated reorganization of AJs could at least partially be rescued by co-expression of a plasmid encoding *AREG::GFP* (Figures 8F and 8F'). Notably, neither AREG knockdown nor its overexpression influenced the expression levels of the ERα target gene *TFF1* (Figures 8D and 8G) showing that AREG acts downstream of ERα in MCF-7 cells.

Given that AREG is a ligand of the EGFR signaling pathway, we finally assessed the role of EGFR in AJ reorganization (Figures 8H and 8I). Indeed, treatment with the selective EGFR tyrosine kinase inhibitor Gefitinib did result in the reorganization of AJs in a dose-dependent manner, albeit less efficiently than with Fulv (Figures 8H and 8H'). Notably, EGFR inhibition did also reduce *AREG* and, to a smaller extent, *TFF1*
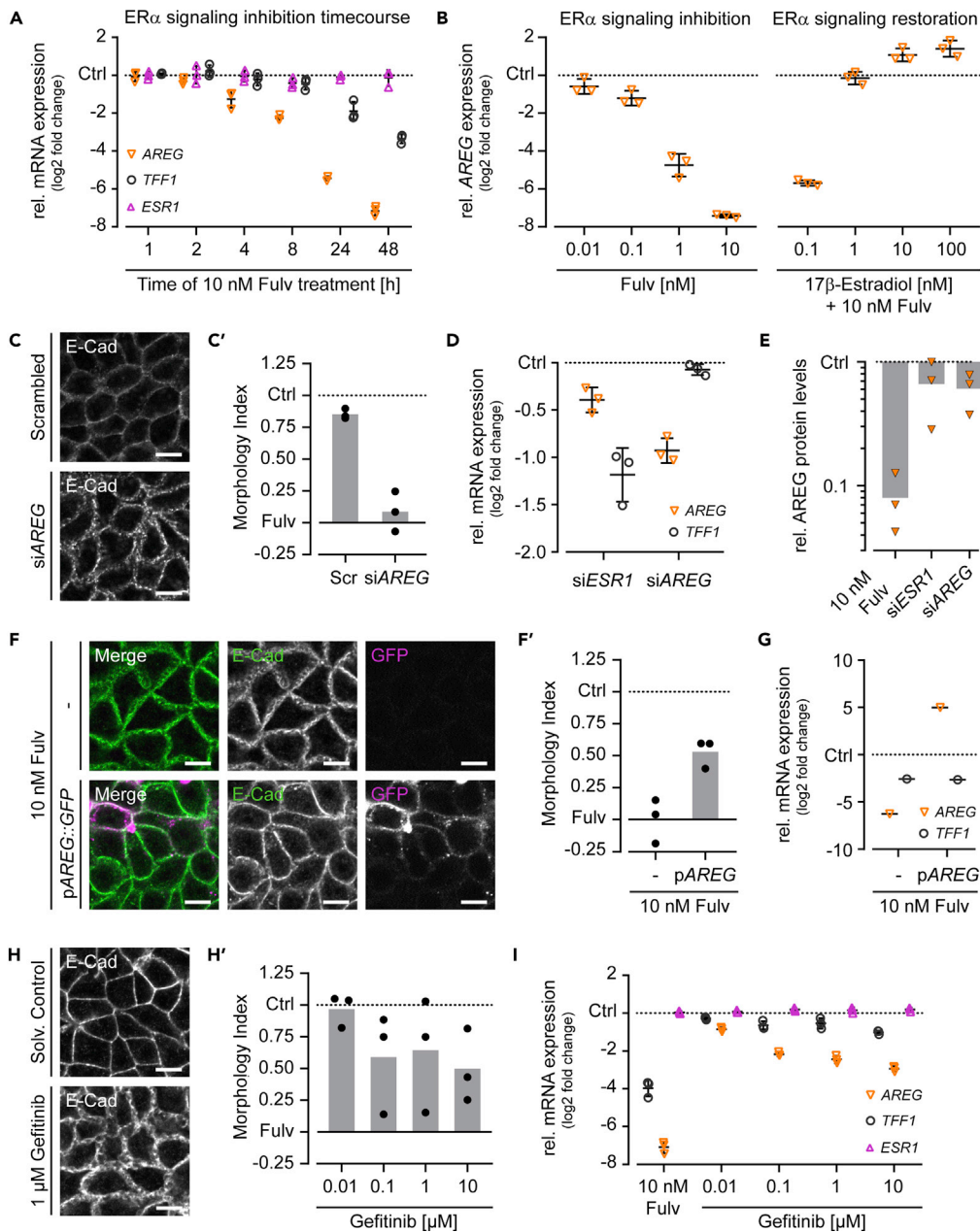
Figure 8. Role of Amphiregulin (AREG) and the Epidermal Growth Factor Receptor (EGFR) Pathway for AJ Reorganization

(A) Time-resolved quantitative RT-PCR measurement of *AREG* (orange) and ERα (*ESR1*, magenta) mRNA expression levels upon Fulv treatment over the course of 48 h. The mRNA expression levels of the ERα target gene *TFF1* serve as readout for ERα signaling activity. Relative mRNA expression levels of each time point are normalized to the corresponding solvent control (Ctrl). Biological replicates, n = 3. Error bars, mean ± SD.

(B) Quantitative RT-PCR measurement of *AREG* (orange) mRNA expression levels upon ERα signaling inhibition (Fulv titration) and restoration (10 nM Fulv in combination with 17β-Estradiol titration) for 48 h (samples from experiment shown in Figure 2A). Relative mRNA expression levels for each treatment condition are normalized to the solvent control (Ctrl). Biological replicates, n = 3. Error bars, mean ± SD.

(C) Immunofluorescence images showing AJ organization (E-Cad) of cells transfected with a pool of four different *AREG* siRNAs in combination as compared with cells transfected with scrambled control siRNA for 72 h. Scale bar, 10 μm.

(C′) Quantification of AJ organization of the experiment shown in (C). The MI is normalized to the negative control (solvent, Ctrl = 1) and positive control (10 nM Fulv, Fulv = 0). Biological replicates, n = 3. Bars, mean of biological replicates.

Figure 8. *Continued*

(D) Quantitative RT-PCR measurement of *AREG* (orange) mRNA expression levels of cells transfected with a pool of four different siRNAs to knockdown ERα (si*ESR1*) and AREG (si*AREG*) for 72 h. The mRNA expression levels of the ERα target gene *TFF1* serve as readout for ERα signaling activity. Relative mRNA expression levels are normalized to the scrambled control (Ctrl). Biological replicates, n = 3. Error bars, mean ± SD.

(E) Western blot analysis and quantification of AREG protein levels upon Fulv treatment (normalized to solvent control, Ctrl), si*ESR1* knockdown, and si*AREG* knockdown (both normalized to scrambled control, Ctrl) for 72 h. Biological replicates, n = 3. Bars, mean of biological replicates.

(F) Immunofluorescence images showing AJ organization (E-Cad, green) in Fulv-treated cells expressing an *AREG::GFP* plasmid (p*AREG::GFP*) for 48 h as compared with untransfected control cells. Transfected cells are visualized by GFP expression (magenta). Scale bar, 10 μm.

(F') Quantification of AJ organization of the experiment shown in (F). The MI is normalized to the negative control (solvent, Ctrl = 1) and positive control (10 nM Fulv, Fulv = 0). The trainings set was generated from reagent control images. Biological replicates, n = 3. Bars, mean of biological replicates.

(G) Quantitative RT-PCR measurement of *AREG* (orange) mRNA expression levels of Fulv-treated cells expressing an *AREG::GFP* plasmid (p*AREG*) for 48 h as compared with untransfected control cells. The mRNA expression levels of the ERα target gene *TFF1* serve as readout for ERα signaling activity. Relative mRNA expression levels are normalized to the reagent control (Ctrl). Biological replicates, n = 1.

(H) Immunofluorescence images showing AJ organization (E-Cad) of cells upon treatment with the EGFR inhibitor Gefitinib for 72 h as compared with solvent control-treated cells. Scale bar, 10 μm.

(H') Quantification of AJ organization of cells upon treatment with different concentrations of the EGFR inhibitor Gefitinib for 72 h as compared with solvent control-treated cells (Ctrl). The MI is normalized to the negative control (solvent, Ctrl = 1) and positive control (10 nM Fulv, Fulv = 0). Biological replicates, n = 3. Bars, mean of biological replicates.

(I) Quantitative RT-PCR measurement of *AREG* (orange) and ERα (*ESR1*, magenta) mRNA expression levels upon Gefitinib treatment for 72 h. The mRNA expression levels of the ERα target gene *TFF1* serve as readout for ERα signaling activity. Relative mRNA expression levels for each treatment condition are normalized to the solvent control (Ctrl). Biological replicates, n = 3. Error bars, mean ± SD.

gene expression levels (Figure 8I) suggesting that the activity of the estrogen signaling pathway was influenced as well. Together, these data delineate a novel mechanism by which the activity of the estrogen signaling pathway controls the organization of AJs through regulating AREG expression. These data also provide first hints for a potential cross talk between the ERα and EGFR signaling pathways during this process, which will need to be addressed in future studies.

DISCUSSION

The etiology of breast cancer development is still largely unknown. One risk factor is the female sex hormone estrogen (Liang and Shang, 2013; Yager and Davidson, 2006). It probably does not trigger the cancer itself but supports its progression. Therefore, adverse health impacts caused by endogenous estrogen levels and environmental chemicals that influence the estrogen system are of high concern (Giulivo et al., 2016). In this study, we describe a novel mechanism of estrogen signaling in controlling adherens junction (AJ) organization and stability in breast cancer cells (Figure 9). According to our model, estrogen-mediated stimulation (estrogenic conditions) or anti-estrogen-mediated inhibition (anti-estrogenic conditions) of ERα signaling remarkably influence the morphology of cell-cell contacts, i.e., the cell membrane shape and the distribution of AJ proteins like E-Cad. This effect is mediated through the activity of the actomyosin network and correlates with functional changes in cell stiffness, stability of AJ, and cell motility. The EGFR ligand AREG is an essential downstream effector of ERα signaling during this AJ reorganization process. Based on this model, our results provide a novel biological mechanism for organizing AJs and thereby influencing the mechanical properties of breast cancer cells. They also provide a new perspective on how estrogens and anti-estrogens might influence the formation of breast tumors. Nevertheless, studies should be encouraged to investigate whether reorganization of AJs can be used as a new functional and potentially clinically relevant endpoint for breast cancer prognosis.

Breast cancer tumorigenesis is a complex multistep process, in which the disturbance of E-Cad-mediated cell-cell adhesion by sustained exposure to estrogens plays an important role. However, a previously described model proposing estrogen-mediated inhibition of E-Cad expression (Cardamone et al., 2009; Oesterreich et al., 2003) might not completely reflect the *in vivo* situation, because E-Cad expression is sustained in the majority of metastatic invasive ductal carcinomas (IDCs), the most common type of breast cancer. In the MCF-7 breast cancer cell line used in this study, ERα signaling activity did not clearly affect E-Cad mRNA expression levels (see Figures 1 and 3) but controlled the distribution of E-Cad along cell membranes and the organization of AJs (see Figures 1, 2, and 4). In case of breast tumor tissue samples from patients with diagnosed IDC,

Estrogenic conditions
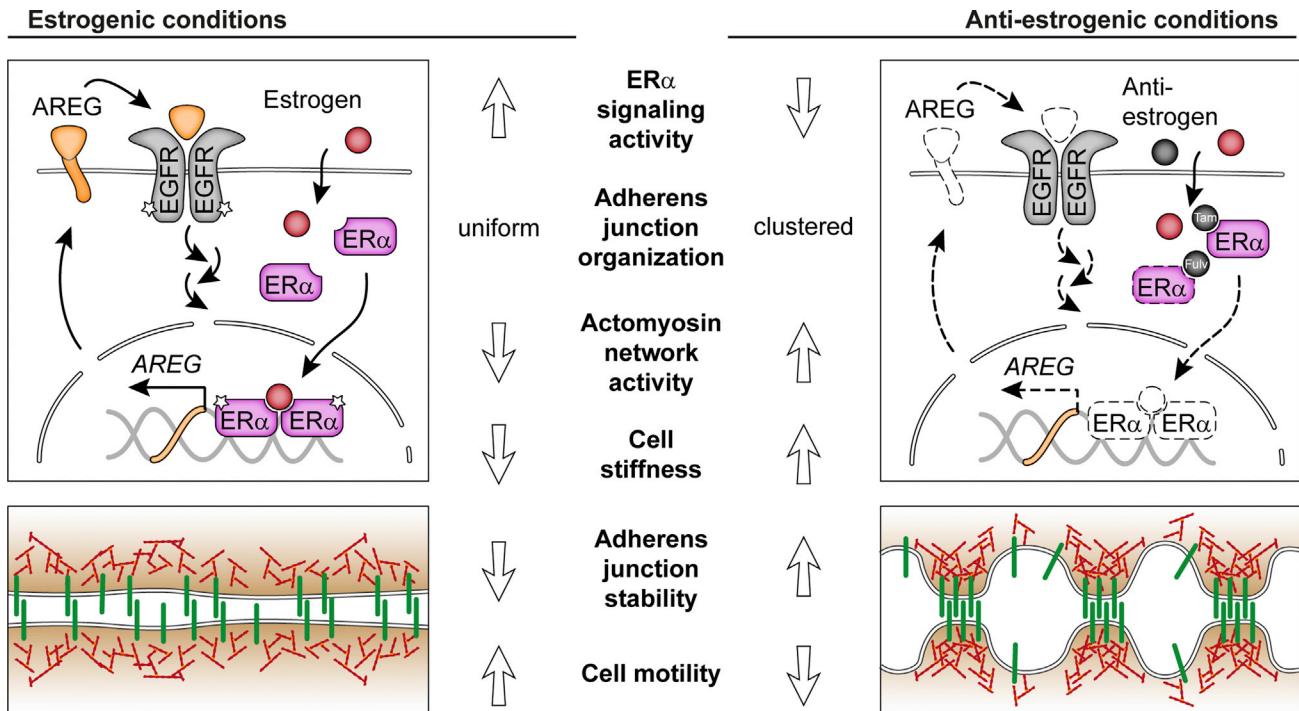
Anti-estrogenic conditions

Figure 9. Working Model Illustrating Mechanistic Events and Functional Consequences that are Involved in Estrogen-Dependent Adherens Junction (AJ) Reorganization

Under estrogenic conditions, ERα monomers bind available estrogens, dimerize, and shuttle to the nucleus to activate target gene expression including *AREG*. Upon processing and secretion of AREG at the cell membrane, it can bind to the Epidermal growth factor receptor (EGFR) and induce further downstream signaling cascades that potentially cross talk with the ERα signaling pathway. Under anti-estrogenic conditions, anti-estrogens perturb ERα signaling activity through different modes of action. Whereas selective estrogen receptor modulators (SERMs) such as Tamoxifen (Tam) only compete with estrogens for receptor binding, selective estrogen receptor degraders (SERDs) like Fulvestrant (Fulv) additionally reduce available ERα protein levels. The inhibition of ERα signaling activity and the corresponding reduction of AREG expression levels eventually lead to the clustering of E-Cad and a striking reorganization of AJs involving the actomyosin cytoskeleton. This change in cell-cell contact architecture further correlates with an increase of cell stiffness and stability of AJs and decrease of cell motility. As these parameters represent functional readouts that are often associated with breast cancer progression and metastasis, the reorganization of AJs may provide a novel functional and clinically relevant endpoint to determine the activity of the estrogen signaling pathway.

variations in the cell membrane distribution of E-Cad were observed including a clustered appearance of E-Cad as seen under anti-estrogenic cell culture conditions (see Figure 5, S1, and S2) suggesting a potential clinical relevance of the estrogen-dependent regulation of AJ organization *in vitro*. Interestingly, our data suggest further that the nuclear localization of ERα per se may not necessarily qualify as a sufficient biomarker for estrogenic activity *in vitro* and *in vivo*. However, future studies using a greater diversity of breast cancer tissue samples and considering more clinical data will be needed to further substantiate these first indications and to explore a potential correlation between AJ organization and breast cancer progression.

To ensure the relevance of the here-proposed endpoint, i.e., AJ reorganization, and the underlying mechanisms, *in vitro* experiments were conducted under physiologically and clinically relevant conditions. MCF-7 breast cancer cells were cultivated in low-estrogen medium containing physiological 17β-Estradiol (E2) levels (3.4–4.1 pM) that were in the range of serum levels of postmenopausal women (Rothman et al., 2011). Furthermore, Fulv-treatment caused cellular responses at concentrations (1–10 nM) that were in the range of steady-state blood plasma levels of patients undergoing anti-estrogen-based endocrine therapy (~20 nM) (McCormack and Sapunar, 2008). The additional application of E2 to Fulv-treated cells restored ERα signaling activity and prevented AJ reorganization at concentrations that would be expected in a competitive situation considering the published ERα-binding affinities of the two compounds (Wakeling et al., 1991).

When exposing breast cancer cells to anti-estrogenic conditions, the cell-cell contact area was strongly reduced along with a discontinuous appearance of AJs and microclustering of E-Cad (see Figure 4). A similar junctional

distribution of vascular endothelial cadherin (VE-Cad) has been observed in distinct endothelial cells of lymphatic capillaries in mice that form functionally specialized button-like intercellular junctions (Baluk et al., 2007). Interestingly, these types of junctions were retained in mature, dermal lymphatic capillaries of mice in the absence of VE-Cad (Hagerling et al., 2018), which aligns with our finding that depletion of E-Cad did not influence the formation of discontinuous AJs in breast cancer cells (see Figure 4). Considering that estrogen receptors are also expressed in vascular endothelial cells, additional studies are needed to identify a potential role of estrogen signaling in regulating junctional distribution of VE-Cad in vascular endothelial cells of the lymphatic and cardiovascular system.

Our data further show that the stability of AJs was increased upon AJ reorganization (see Figure 7). This effect can most likely be attributed to the concomitant formation of E-Cad microclusters since clustering of E-Cad into micron-scaled assemblies has been shown to promote the stability of AJs and the strength of cell-cell adhesion (Yap et al., 2015). Our model suggesting that ERα signaling does not modulate cell-cell adhesion through regulating E-Cad expression but rather through E-Cad membrane distribution and AJ organization is further in line with previous data showing that the adhesiveness of different cell lines does not necessarily correlate with E-Cad expression levels (Omidvar et al., 2014).

At AJs, E-Cad is the central hub integrating cell-cell adhesion and actomyosin-based contractility through catenins (Lecuit and Yap, 2015). In our experiments, α-Catenin, β-Catenin, and p120-Catenin were, along with E-Cad and F-Actin, still detectable at reorganized AJs upon anti-estrogen treatment (see Figure S1) indicating that AJ composition remained intact. In line with published data demonstrating the relevance of the actomyosin network for AJ formation, organization, and stability (Hong et al., 2013; Smutny et al., 2010; Vasioukhin et al., 2000), the anti-estrogen-induced reorganization of AJs could be reverted by manipulating actomyosin network activity (see Figures 6 and S3). In comparison with studies using other MCF-7 variants that also demonstrate the influence of ERα signaling on the actomyosin network (DePasquale, 1999; DePasquale et al., 1994; Huan et al., 2014), our data now provide a more detailed understanding of the mechanistic consequences of estrogen signaling in breast cancer cells, namely, the regulation of AJ organization and stability.

Furthermore, here we show that anti-estrogen-mediated modulation of the actomyosin network activity affected the mechanical properties of breast cancer cells, i.e., causing an increase in cell stiffness, as measured by AFM (apparent Young's moduli [Radmacher, 2002]) (see Figure 6). In support of the validity of our data, the stiffness of cells under estrogenic conditions was generally in the range of values recently reported for other MCF-7 subclones (Li et al., 2008; Omidvar et al., 2014). The concomitant increase of cell stiffness and AJ stability upon anti-estrogen treatment is also in agreement with previously published data demonstrating a strong positive correlation between cell stiffness and cell-cell adhesion *in vitro* (Omidvar et al., 2014). Considering that, in other *in vitro* and *in vivo* studies, reduced cell stiffness correlated with increased malignity of breast tumors (Guck et al., 2005; Li et al., 2008; Nikkhah et al., 2011; Plodinec et al., 2012), the here-observed increase of cell stiffness under anti-estrogenic conditions supports the potential clinical relevance of the data collected in this study. As a functional consequence of ERα signaling inhibition, the motility of breast cancer cells within the cellular monolayer was also found to be decreased (see Figure 7), which is in line with the previous findings that stimulation of ERα signaling drives breast cancer cell motility through actomyosin network reorganization *in vitro* (Giretti et al., 2008; Sanchez et al., 2010; Zheng et al., 2011). The effects of estrogenic activity on cell stiffness, AJ stability, and cell motility represent important functional parameters with a clear clinical relevance in breast cancer metastasis.

Our data also delineate a novel mechanism in which ERα signaling controls AJ organization and stability through regulation of Amphiregulin (AREG), a member of the epidermal growth factor receptor (EGFR) pathway (see Figure 8). It is well known that ERα signaling through AREG/EGFR plays an essential role in the regulation of mammary gland development. Multiple knockdown studies in mice demonstrated that pubertal outgrowth of the ductal epithelium was impaired upon depletion of ERα (Mallepell et al., 2006), AREG (Ciarloni et al., 2007; Luetteke et al., 1999), or EGFR (Wiesen et al., 1999). In this study, we have shown that the functional depletion of any of these key players by treatment with inhibitors or siRNA knockdown also caused a morphological change in epithelial architecture, i.e., reorganization of AJs, in breast cancer cells. To what extent the reorganization of AJs might relate to the impaired ductal outgrowth observed *in vivo* or relates to it, however, remains to be addressed.

In addition, AREG is known to play a central role in tumor development and resistance to cancer treatments. AREG regulates cell proliferation, migration, and invasion as well as cancer cell stemness as a

mediator of the Hippo pathway (Busser et al., 2011; Park et al., 2018; Willmarth and Ethier, 2006; Zhang et al., 2009). A strong increase in AREG expression along with elevated expression of ERα could be observed in premalignant hyperplastic precursors already during the early phase of breast cancer development (Lee et al., 2007). Importantly, AREG is also frequently overexpressed in ERα-positive human breast tumors at the mRNA and protein levels and suppressed in patients undergoing endocrine therapy (Peterson et al., 2015). In this study, we have shown that *AREG* is also a transcriptional target and critical downstream effector gene of ERα in regulating AJ organization *in vitro* supporting the clinical relevance of these mechanistic data (see Figure 8). These data further agree with the reduction of *AREG* mRNA expression upon anti-estrogen treatment that was observed in another variant of the MCF-7 cell line (Martinez-Lacaci et al., 1995) and with the identification of functional estrogen response element (ERE) sites around the *AREG* transcription start site *in vitro* (Britton et al., 2006) and *in vivo* (McBryan et al., 2007).

Moreover, it has been shown that exogenous administration of AREG restored mammary gland development in ERα knockdown mice, which was, however, not the case for estradiol stimulation of ovariectomized AREG knockdown mice (Ciarloni et al., 2007). Notably, the proliferative capacity of AREG knockdown cells could be retained when transplanted into wild-type epithelial cells expressing AREG (Ciarloni et al., 2007). This apparent juxtacrine/paracrine mechanism of AREG release is in line with our finding that anti-estrogen-mediated AJ reorganization could even be relieved throughout the cellular monolayer when AREG expression was only restored in a subset of cells by AREG::GFP overexpression (see Figure 8).

Notably, *AREG* mRNA expression levels were likewise reduced upon Gefitinib-mediated EGFR inhibition (see Figure 8) suggesting that AREG expression is also regulated by the EGFR signaling pathway. Indeed, such a bidirectional cross talk between EGFR and ERα signaling has already been proposed by another study showing that phosphorylation of ERα at S118 was reduced in response to Gefitinib treatment (Britton et al., 2006). Future studies focusing on the potential cross talk between EGFR and ERα signaling will provide deeper insights into its role for AJ organization and stability in breast cancer development.

In conclusion, our data on the estrogen-dependent spatial reorganization of AJs open up the possibility to better understand the biomechanical properties of cell-cell contacts in epithelial tissues. They provide a starting point for future studies that investigate to what extend these effects can also be detected in other cancer cell lines or in normal epithelial cells. Particularly, estrogen sensitivity of cadherin-based cell junctions may explain the observed gender and age-specific influences of estrogens on cardiovascular function and disease (Mendelsohn and Karas, 2005; Murphy, 2011; Novella et al., 2012). Moreover, the specificity of AJ reorganization to the ERα signaling pathway, and its dose-dependent regulation, makes it an ideal functional endpoint for measuring estrogenic and anti-estrogenic activity in breast cancer cells. Thus, we developed an *in vitro* assay (Kornhuber et al., under review), which allows robust and reliable identification of chemical compounds with estrogenic and anti-estrogenic potential (e.g., for drug discovery or characterization of environmental chemicals). We believe that a detailed characterization of AJ organization and E-Cad distribution can be a valuable other key event in breast cancer diagnostics and monitoring of anti-estrogenic therapy, as the expression rates of E-Cad and the localization of ERα may not be enough reliable biomarkers for breast cancer metastasis.

Limitations of the Study

The estrogen-dependent organization of AJs was observed in two distinct MCF-7 cell lines. These findings provide a starting point for further analyses that assess to which degree these findings are generalizable to a greater diversity of other breast cancer cell lines and normal mammary epithelial cells. Moreover, the validation of these *in vitro* findings in human breast tumor tissue samples would further benefit from more advanced image analysis pipelines, e.g., involving artificial intelligence, that allow their reliable segmentation and classification using suitable reference material. Finally, although AREG/EGFR signaling was necessary and sufficient for ERα-dependent AJ organization, the precise molecular mechanisms that specifically connect these two signaling pathways and the actomyosin cytoskeleton remain to be identified.

Resource Availability

Lead Contact

Further information and requests for resources and reagents should be directed to and will be fulfilled by the Lead Contact, Prof. Dr. Gilbert Schönfelder (gilbert.schoenfelder@bfr.bund.de).

Materials Availability

This study did not generate new unique reagents.

Data and Code Availability

Customized image analysis pipelines have been generated using the CellProfiler (Carpenter et al., 2006) and CellProfiler Analyst (Jones et al., 2008) software packages and are available upon request.

METHODS

All methods can be found in the accompanying Transparent Methods supplemental file.

SUPPLEMENTAL INFORMATION

Supplemental Information can be found online at https://doi.org/10.1016/j.isci.2020.101683.

AUTHOR CONTRIBUTIONS

P.B., M.K., S.D., M.O., and G.S. designed experiments. M.K., P.B., S.D., and J.Z. collected and analyzed the data. A.V.T. and J.G. performed and analyzed AFM experiments. B.F. and T.M. performed and analyzed TEM experiments. S.D., P.B., M.K., M.O., and G.S. wrote the manuscript and all remaining authors provided detailed comments.

DECLARATION OF INTERESTS

A European (EP 3517967 A1) and international (PCT) (WO 2019145517 A1) patent application for the use of the here-described endpoint (estrogen-dependent reorganization of adherens junctions) to screen substances for estrogenic or anti-estrogenic activity has been filed at the European Patent Office by the employer (German Federal Institute for Risk Assessment [BfR]) of the following authors: P.B., M.K., S.D., M.O., and G.S.. The German Federal Institute for Risk Assessment (BfR) is a scientifically independent institution within the portfolio of the Federal Ministry of Food and Agriculture (BMEL) in Germany. The authors' freedom to design, conduct, interpret, and publish research is explicitly not compromised. All remaining authors do not have any competing financial interests.

REFERENCES

Baluk, P., Fuxe, J., Hashizume, H., Romano, T., Lashnits, E., Butz, S., Vestweber, D., Corada, M., Molendini, C., Dejana, E., et al. (2007). Functionally specialized junctions between endothelial cells of lymphatic vessels. J. Exp. Med. *204*, 2349–2362.

Berx, G., and van Roy, F. (2009). Involvement of members of the cadherin superfamily in cancer. Cold Spring Harb. Perspect. Biol. *1*, a003129.

Britton, D.J., Hutcheson, I.R., Knowlden, J.M., Barrow, D., Giles, M., McClelland, R.A., Gee, J.M., and Nicholson, R.I. (2006). Bidirectional cross talk between ERalpha and EGFR signalling pathways regulates tamoxifen-resistant growth. Breast Cancer Res. Treat. *96*, 131–146.

Busser, B., Sancey, L., Brambilla, E., Coll, J.L., and Hurbin, A. (2011). The multiple roles of amphiregulin in human cancer. Biochim. Biophys. Acta *1816*, 119–131.

Cardamone, M.D., Bardella, C., Gutierrez, A., Di Croce, L., Rosenfeld, M.G., Di Renzo, M.F., and De Bortoli, M. (2009). ERalpha as ligand-independent activator of CDH-1 regulates determination and maintenance of epithelial morphology in breast cancer cells. Proc. Natl. Acad. Sci. U S A *106*, 7420–7425.

Carpenter, A.E., Jones, T.R., Lamprecht, M.R., Clarke, C., Kang, I.H., Friman, O., Guertin, D.A., Chang, J.H., Lindquist, R.A., Moffat, J., et al.

(2006). CellProfiler: image analysis software for identifying and quantifying cell phenotypes. Genome Biol. *7*, R100.

Ciarloni, L., Mallepell, S., and Brisken, C. (2007). Amphiregulin is an essential mediator of estrogen receptor alpha function in mammary gland development. Proc. Natl. Acad. Sci. U S A *104*, 5455–5460.

de Beco, S., Gueudry, C., Amblard, F., and Coscoy, S. (2009). Endocytosis is required for E-cadherin redistribution at mature adherens junctions. Proc. Natl. Acad. Sci. U S A *106*, 7010–7015.

Denkert, C., Bucher, E., Hilvo, M., Salek, R., Oresic, M., Griffin, J., Brockmoller, S., Klauschen, F., Loibl, S., Barupal, D.K., et al. (2012). Metabolomics of human breast cancer: new approaches for tumor typing and biomarker discovery. Genome Med. *4*, 37.

DePasquale, J.A. (1999). Rearrangement of the F-actin cytoskeleton in estradiol-treated MCF-7 breast carcinoma cells. Histochem. Cell Biol. *112*, 341–350.

DePasquale, J.A., Samsonoff, W.A., and Gierthy, J.F. (1994). 17-beta-Estradiol induced alterations of cell-matrix and intercellular adhesions in a human mammary carcinoma cell line. J. Cell Sci. *107* (Pt 5), 1241–1254.

Early Breast Cancer Trialists' Collaborative Group (EBCTCG), Davies, C., Godwin, J., Gray, R., Clarke, M., Cutter, D., Darby, S., McGale, P., Pan, H.C., Taylor, C., et al. (2011). Relevance of breast cancer hormone receptors and other factors to the efficacy of adjuvant tamoxifen: patient-level meta-analysis of randomised trials. Lancet *378*, 771–784.

Fujita, N., Jaye, D.L., Kajita, M., Geigerman, C., Moreno, C.S., and Wade, P.A. (2003). MTA3, a Mi-2/NuRD complex subunit, regulates an invasive growth pathway in breast cancer. Cell *113*, 207–219.

Giretti, M.S., Fu, X.D., De Rosa, G., Sarotto, I., Baldacci, C., Garibaldi, S., Mannella, P., Biglia, N., Sismondi, P., Genazzani, A.R., et al. (2008). Extra-nuclear signalling of estrogen receptor to breast cancer cytoskeletal remodelling, migration and invasion. PLoS One *3*, e2238.

Giulivo, M., Lopez de Alda, M., Capri, E., and Barcelo, D. (2016). Human exposure to endocrine disrupting compounds: their role in reproductive systems, metabolic syndrome and breast cancer. A review. Environ. Res. *151*, 251–264.

Guck, J., Schinkinger, S., Lincoln, B., Wottawah, F., Ebert, S., Romeyke, M., Lenz, D., Erickson, H.M., Ananthakrishnan, R., Mitchell, D., et al. (2005). Optical deformability as an inherent cell marker for testing malignant transformation and metastatic competence. Biophys. J. *88*, 3689–3698.

Hagerling, R., Hoppe, E., Dierkes, C., Stehling, M., Makinen, T., Butz, S., Vestweber, D., and Kiefer, F. (2018). Distinct roles of VE-cadherin for development and maintenance of specific lymph vessel beds. EMBO J. *37*, e98271.

Hashizume, R., Koizumi, H., Ihara, A., Ohta, T., and Uchikoshi, T. (1996). Expression of beta-catenin in normal breast tissue and breast carcinoma: a comparative study with epithelial cadherin and alpha-catenin. Histopathology *29*, 139–146.

Herbst, A.L., Ulfelder, H., and Poskanzer, D.C. (1971). Adenocarcinoma of the vagina. Association of maternal stilbestrol therapy with tumor appearance in young women. N. Engl. J. Med. *284*, 878–881.

Hofmann, D., Nitz, U., Gluz, O., Kates, R.E., Schinkoethe, T., Staib, P., and Harbeck, N. (2013). WSG ADAPT - adjuvant dynamic marker-adjusted personalized therapy trial optimizing risk assessment and therapy response prediction in early breast cancer: study protocol for a prospective, multi-center, controlled, non-blinded, randomized, investigator initiated phase II/III trial. Trials *14*, 261.

Hong, S., Troyanovsky, R.B., and Troyanovsky, S.M. (2013). Binding to F-actin guides cadherin cluster assembly, stability, and movement. J. Cell Biol. *201*, 131–143.

Hoover, R.N., Hyer, M., Pfeiffer, R.M., Adam, E., Bond, B., Cheville, A.L., Colton, T., Hartge, P., Hatch, E.E., Herbst, A.L., et al. (2011). Adverse health outcomes in women exposed in utero to diethylstilbestrol. N. Engl. J. Med. *365*, 1304–1314.

Huan, J., Wang, L., Xing, L., Qin, X., Feng, L., Pan, X., and Zhu, L. (2014). Insights into significant pathways and gene interaction networks underlying breast cancer cell line MCF-7 treated with 17beta-estradiol (E2). Gene *533*, 346–355.

Huang, B., Omoto, Y., Iwase, H., Yamashita, H., Toyama, T., Coombes, R.C., Filipovic, A., Warner, M., and Gustafsson, J.A. (2014). Differential expression of estrogen receptor alpha, beta1, and beta2 in lobular and ductal breast cancer. Proc. Natl. Acad. Sci. U S A *111*, 1933–1938.

Jones, T.R., Kang, I.H., Wheeler, D.B., Lindquist, R.A., Papallo, A., Sabatini, D.M., Golland, P., and Carpenter, A.E. (2008). CellProfiler Analyst: data exploration and analysis software for complex image-based screens. BMC Bioinformatics *9*, 482.

Lecuit, T., and Yap, A.S. (2015). E-cadherin junctions as active mechanical integrators in tissue dynamics. Nat. Cell Biol. *17*, 533–539.

Lee, C.I., Goodwin, A., and Wilcken, N. (2017). Fulvestrant for hormone-sensitive metastatic breast cancer. Cochrane Database Syst. Rev. *1*, CD011093.

Lee, S., Medina, D., Tsimelzon, A., Mohsin, S.K., Mao, S., Wu, Y., and Allred, D.C. (2007). Alterations of gene expression in the development of early hyperplastic precursors of breast cancer. Am. J. Pathol. *171*, 252–262.

Li, Q.S., Lee, G.Y., Ong, C.N., and Lim, C.T. (2008). AFM indentation study of breast cancer cells. Biochem. Biophys. Res. Commun. *374*, 609–613.

Liang, J., and Shang, Y. (2013). Estrogen and cancer. Annu. Rev. Physiol. *75*, 225–240.

List, H.J., Lauritsen, K.J., Reiter, R., Powers, C., Wellstein, A., and Riegel, A.T. (2001). Ribozyme targeting demonstrates that the nuclear receptor coactivator AIB1 is a rate-limiting factor for estrogen-dependent growth of human MCF-7 breast cancer cells. J. Biol. Chem. *276*, 23763–23768.

Luetteke, N.C., Qiu, T.H., Fenton, S.E., Troyer, K.L., Riedel, R.F., Chang, A., and Lee, D.C. (1999). Targeted inactivation of the EGF and amphiregulin genes reveals distinct roles for EGF receptor ligands in mouse mammary gland development. Development *126*, 2739–2750.

Mallepell, S., Krust, A., Chambon, P., and Brisken, C. (2006). Paracrine signaling through the epithelial estrogen receptor alpha is required for proliferation and morphogenesis in the mammary gland. Proc. Natl. Acad. Sci. U S A *103*, 2196–2201.

Martinez-Lacaci, I., Saceda, M., Plowman, G.D., Johnson, G.R., Normanno, N., Salomon, D.S., and Dickson, R.B. (1995). Estrogen and phorbol esters regulate amphiregulin expression by two separate mechanisms in human breast cancer cell lines. Endocrinology *136*, 3983–3992.

Maximov, P.Y., McDaniel, R.E., and Jordan, V.C. (2013). Tamoxifen: Pioneering Medicine in Breast Cancer (Springer).

McBryan, J., Howlin, J., Kenny, P.A., Shioda, T., and Martin, F. (2007). ERalpha-CITED1 co-regulated genes expressed during pubertal mammary gland development: implications for breast cancer prognosis. Oncogene *26*, 6406–6419.

McBryan, J., Howlin, J., Napoletano, S., and Martin, F. (2008). Amphiregulin: role in mammary gland development and breast cancer. J. Mammary Gland Biol. Neoplasia *13*, 159–169.

McCormack, P., and Sapunar, F. (2008). Pharmacokinetic profile of the fulvestrant loading dose regimen in postmenopausal women with hormone receptor-positive advanced breast cancer. Clin. Breast Cancer *8*, 347–351.

Mendelsohn, M.E., and Karas, R.H. (2005). Molecular and cellular basis of cardiovascular gender differences. Science *308*, 1583–1587.

Murphy, E. (2011). Estrogen signaling and cardiovascular disease. Circ. Res. *109*, 687–696.

Nelson, W.J. (2008). Regulation of cell-cell adhesion by the cadherin-catenin complex. Biochem. Soc. Trans. *36*, 149–155.

Nikkhah, M., Strobl, J.S., Schmelz, E.M., and Agah, M. (2011). Evaluation of the influence of growth medium composition on cell elasticity. J. Biomech. *44*, 762–766.

Novella, S., Dantas, A.P., Segarra, G., Medina, P., and Hermenegildo, C. (2012). Vascular aging in women: is estrogen the fountain of youth? Front. Physiol. *3*, 165.

Oesterreich, S., Deng, W., Jiang, S., Cui, X., Ivanova, M., Schiff, R., Kang, K., Hadsell, D.L., Behrens, J., and Lee, A.V. (2003). Estrogen-mediated down-regulation of E-cadherin in breast cancer cells. Cancer Res. *63*, 5203–5208.

Omidvar, R., Tafazzoli-Shadpour, M., Shokrgozar, M.A., and Rostami, M. (2014). Atomic force microscope-based single cell force spectroscopy of breast cancer cell lines: an approach for evaluating cellular invasion. J. Biomech. *47*, 3373–3379.

Park, J.H., Shin, J.E., and Park, H.W. (2018). The role of Hippo pathway in cancer stem cell biology. Mol. Cell 41, 83–92.

Peterson, E.A., Jenkins, E.C., Lofgren, K.A., Chandiramani, N., Liu, H., Aranda, E., Barnett, M., and Kenny, P.A. (2015). Amphiregulin is a critical downstream effector of estrogen signaling in ERalpha-positive breast cancer. Cancer Res. 75, 4830–4838.

Plodinec, M., Loparic, M., Monnier, C.A., Obermann, E.C., Zanetti-Dallenbach, R., Oertle, P., Hyotyla, J.T., Aebi, U., Bentires-Alj, M., Lim, R.Y., et al. (2012). The nanomechanical signature of breast cancer. Nat. Nanotechnol. 7, 757–765.

Qureshi, H.S., Linden, M.D., Divine, G., and Raju, U.B. (2006). E-cadherin status in breast cancer correlates with histologic type but does not correlate with established prognostic parameters. Am. J. Clin. Pathol. 125, 377–385.

Radmacher, M. (2002). Measuring the elastic properties of living cells by the atomic force microscope. Methods Cell Biol. 68, 67–90.

Rothman, M.S., Carlson, N.E., Xu, M., Wang, C., Swerdloff, R., Lee, P., Goh, V.H., Ridgway, E.C., and Wierman, M.E. (2011). Reexamination of testosterone, dihydrotestosterone, estradiol and estrone levels across the menstrual cycle and in postmenopausal women measured by liquid chromatography-tandem mass spectrometry. Steroids 76, 177–182.

Sanchez, A.M., Flamini, M.I., Baldacci, C., Goglia, L., Genazzani, A.R., and Simoncini, T. (2010). Estrogen receptor-alpha promotes breast cancer cell motility and invasion via focal adhesion kinase and N-WASP. Mol. Endocrinol. 24, 2114–2125.

Smutny, M., Cox, H.L., Leerberg, J.M., Kovacs, E.M., Conti, M.A., Ferguson, C., Hamilton, N.A.,

Parton, R.G., Adelstein, R.S., and Yap, A.S. (2010). Myosin II isoforms identify distinct functional modules that support integrity of the epithelial zonula adherens. Nat. Cell Biol. 12, 696–702.

Tecalco-Cruz, A.C., Perez-Alvarado, I.A., Ramirez-Jarquin, J.O., and Rocha-Zavaleta, L. (2017). Nucleo-cytoplasmic transport of estrogen receptor alpha in breast cancer cells. Cell Signal. 34, 121–132.

Thomas, C., and Gustafsson, J.A. (2011). The different roles of ER subtypes in cancer biology and therapy. Nat. Rev. Cancer 11, 597–608.

Vasioukhin, V., Bauer, C., Yin, M., and Fuchs, E. (2000). Directed actin polymerization is the driving force for epithelial cell-cell adhesion. Cell 100, 209–219.

Villalobos, M., Olea, N., Brotons, J.A., Olea-Serrano, M.F., Ruiz de Almodovar, J.M., and Pedraza, V. (1995). The E-screen assay: a comparison of different MCF7 cell stocks. Environ. Health Perspect. 103, 844–850.

Wakeling, A.E., Dukes, M., and Bowler, J. (1991). A potent specific pure antiestrogen with clinical potential. Cancer Res. 51, 3867–3873.

Wellings, S.R., and Jensen, H.M. (1973). On the origin and progression of ductal carcinoma in the human breast. J. Natl. Cancer Inst. 50, 1111–1118.

Wiesen, J.F., Young, P., Werb, Z., and Cunha, G.R. (1999). Signaling through the stromal epidermal growth factor receptor is necessary for mammary ductal development. Development 126, 335–344.

C.P. Wild, E. Weiderpass, and B.W. Stewart, eds. (2020). World Cancer Report: Cancer Research for Cancer Prevention (International Agency for Research on Cancer), Licence: CC BY-NC-ND 3.0 IGO. http://publications.iarc.fr/586.

Willmarth, N.E., and Ethier, S.P. (2006). Autocrine and juxtacrine effects of amphiregulin on the proliferative, invasive, and migratory properties of normal and neoplastic human mammary epithelial cells. J. Biol. Chem. 281, 37728–37737.

Yager, J.D., and Davidson, N.E. (2006). Estrogen carcinogenesis in breast cancer. N. Engl. J. Med. 354, 270–282.

Yap, A.S., Gomez, G.A., and Parton, R.G. (2015). Adherens junctions revisualized: organizing cadherins as nanoassemblies. Dev. Cell 35, 12–20.

Ye, X., and Weinberg, R.A. (2015). Epithelial-mesenchymal plasticity: a central regulator of cancer progression. Trends Cell Biol. 25, 675–686.

Ye, Y., Xiao, Y., Wang, W., Yearsley, K., Gao, J.X., and Barsky, S.H. (2008). ERalpha suppresses slug expression directly by transcriptional repression. Biochem. J. 416, 179–187.

Ye, Y., Xiao, Y., Wang, W., Yearsley, K., Gao, J.X., Shetuni, B., and Barsky, S.H. (2010). ERalpha signaling through slug regulates E-cadherin and EMT. Oncogene 29, 1451–1462.

Zhang, J., Ji, J.Y., Yu, M., Overholtzer, M., Smolen, G.A., Wang, R., Brugge, J.S., Dyson, N.J., and Haber, D.A. (2009). YAP-dependent induction of amphiregulin identifies a non-cell-autonomous component of the Hippo pathway. Nat. Cell Biol. 11, 1444–1450.

Zheng, S., Huang, J., Zhou, K., Zhang, C., Xiang, Q., Tan, Z., Wang, T., and Fu, X. (2011). 17beta-Estradiol enhances breast cancer cell motility and invasion via extra-nuclear activation of actin-binding protein ezrin. PLoS One 6, e22439.

Supplemental Information

Estrogens Determine Adherens Junction

Organization and E-Cadherin Clustering

in Breast Cancer Cells via Amphiregulin

Philip Bischoff, Marja Kornhuber, Sebastian Dunst, Jakob Zell, Beatrix Fauler, Thorsten Mielke, Anna V. Taubenberger, Jochen Guck, Michael Oelgeschläger, and **Gilbert Schönfelder**

Supplemental figures

A

	E-Cad	β-Catenin	α-Catenin	p120-Catenin	F-Actin
Solv. control					
10 nM Fulv	E-Cad	β-Catenin	α-Catenin	p120-Catenin	F-Actin

B Selective Estrogen Receptor Degrader (SERD)

Solv. control — Merge / E-Cad / ERα
100 nM ZK164015 (48h) — Merge / E-Cad / ERα

C Selective Estrogen Receptor Modulator (SERM)

Solv. control — Merge / E-Cad / ERα
1 μM Tam (144h) — Merge / E-Cad / ERα

D

Solv. control — E-Cad
Selective Estrogen Receptor β Antagonist
10 nM PHTPP / 1 μM PHTPP
10 nM Fulv — E-Cad / E-Cad / E-Cad

E

HCT116 — Empty vector / pERα / pERβ
MCF-7 vBOS — Solv. Control / 10 nM Fulv
MCF-7 E-Cad-GFP — Solv. Control / 10 nM Fulv

ERβ (56 kDa)
ERα (66 kDa)
Loading control

F Breast cancer sections (ADAPT trial)

ADAPT-009 (region 1) — Merge / E-Cad / ERα
ADAPT-032 (region 1) — Merge / E-Cad / ERα
ADAPT-013* (region 1) — Merge / E-Cad / ERα

ADAPT-009 (region 2) — Merge / E-Cad / ERα
ADAPT-032 (region 2) — Merge / E-Cad / ERα
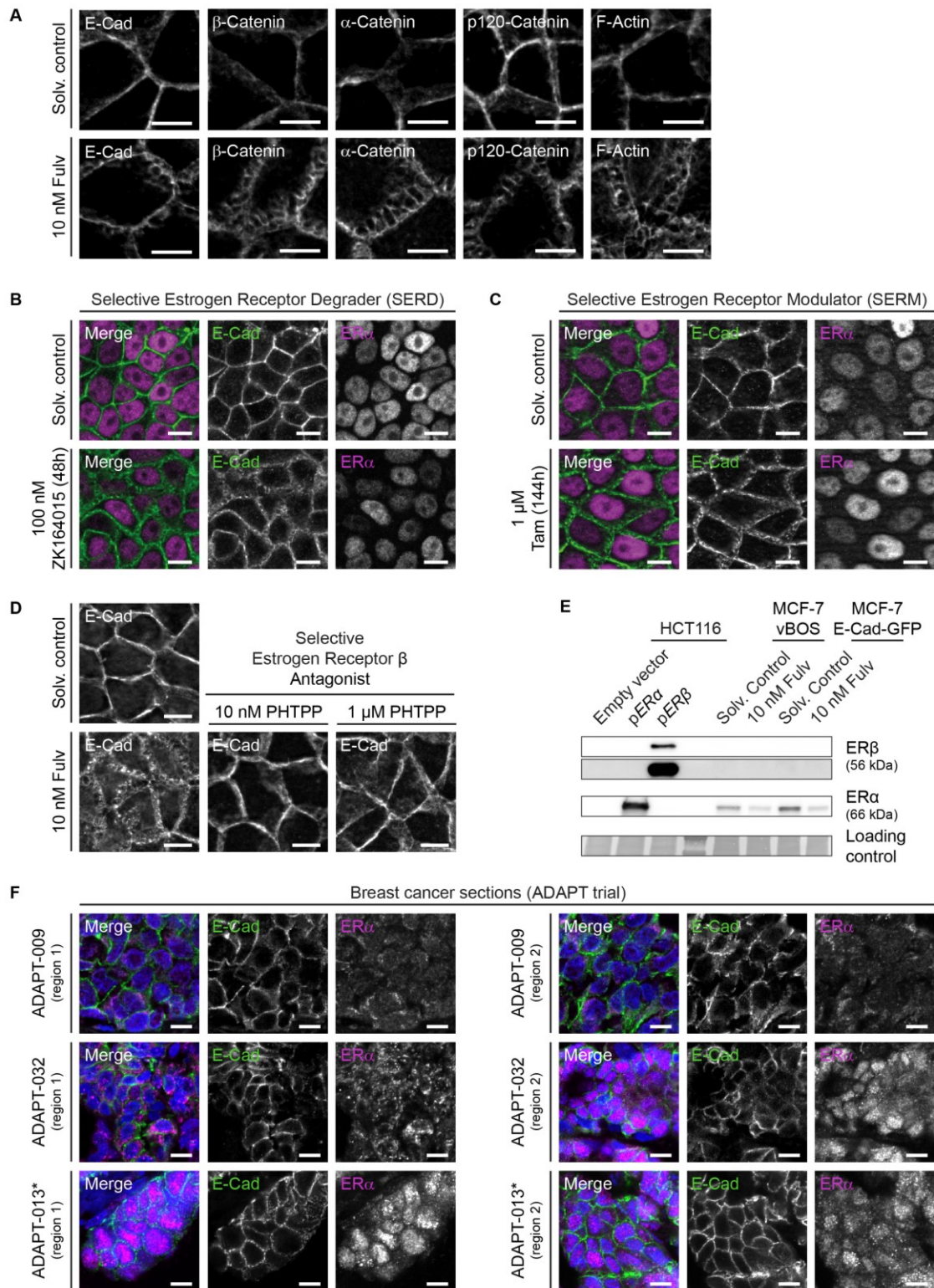ADAPT-013* (region 2) — Merge / E-Cad / ERα

Figure S1 (Related to Figure 1 and Figure 5, Table 1 and Table 2) Adherens junction (AJ) organization upon modulation of ERα and ERβ signaling. AJ organization and ERα localization in breast tumor tissue samples from ADAPT trial.

(A) Immunofluorescence images showing organization of AJ components including the cytoplasmic adaptor proteins α-Catenin, β-Catenin and p120-Catenin connecting E-Cad to the underlying actomyosin network (F-Actin) upon Fulv treatment for 48 hours compared to the solvent control. Scale bar, 10 μm.

(B-C) Immunofluorescence images showing AJ organization (E-Cad, green) and ERα levels (magenta) upon treatment with the selective estrogen receptor degrader (SERD) ZK164015 for 48 hours and treatment with the selective estrogen receptor modulator (SERM) Tamoxifen (Tam) for 144 hours as compared to the solvent control. Scale bar, 10 μm.

(D) Immunofluorescence images showing AJ organization (E-Cad) of cells upon treatment with the selective estrogen receptor β antagonist PHTPP for 48 hours as compared to Fulv and solvent control-treated cells. Scale bar, 10 μm.

(E) Representative western blot showing ERα and ERβ expression status of MCF-7/vBOS and MCF-7/Ecad-GFP cells treated with Fulv or solvent control as compared to HCT116 colon carcinoma cells overexpressing ERα and ERβ. Loading control, Coomassie total protein staining.

(F) Immunofluorescence images showing AJ organization (E-Cad, green) and ERα localization (magenta) in breast tumor tissue samples from patients with diagnosed invasive ductal carcinoma (IDC). An asterisk indicates sections with clustered appearance of E-Cad along cell membranes. Samples obtained from ADAPT trial (results summarized in table 2). The numbers of histological sections were anonymized. Scale bar, 10 μm.

A Breast cancer sections (METAcancer project)

META-83 — Merge | E-Cad | ERα
META-292 — Merge | E-Cad | ERα
META-100 — Merge | E-Cad | ERα
META-23* — Merge | E-Cad | ERα
META-228 — Merge | E-Cad | ERα
META-450* — Merge | E-Cad | ERα
META-240 — Merge | E-Cad | ERα
META-280* — Merge | E-Cad | ERα

META-321 — Merge | E-Cad | ERα
META-357 — Merge | E-Cad | ERα
META-365* — Merge | E-Cad | ERα
META-327 — Merge | E-Cad | ERα
META-222 — Merge | E-Cad | ERα
META-102 — Merge | E-Cad | ERα
META-204 — Merge | E-Cad | ERα
META-277 — Merge | E-Cad | ERα

B

Scrambled

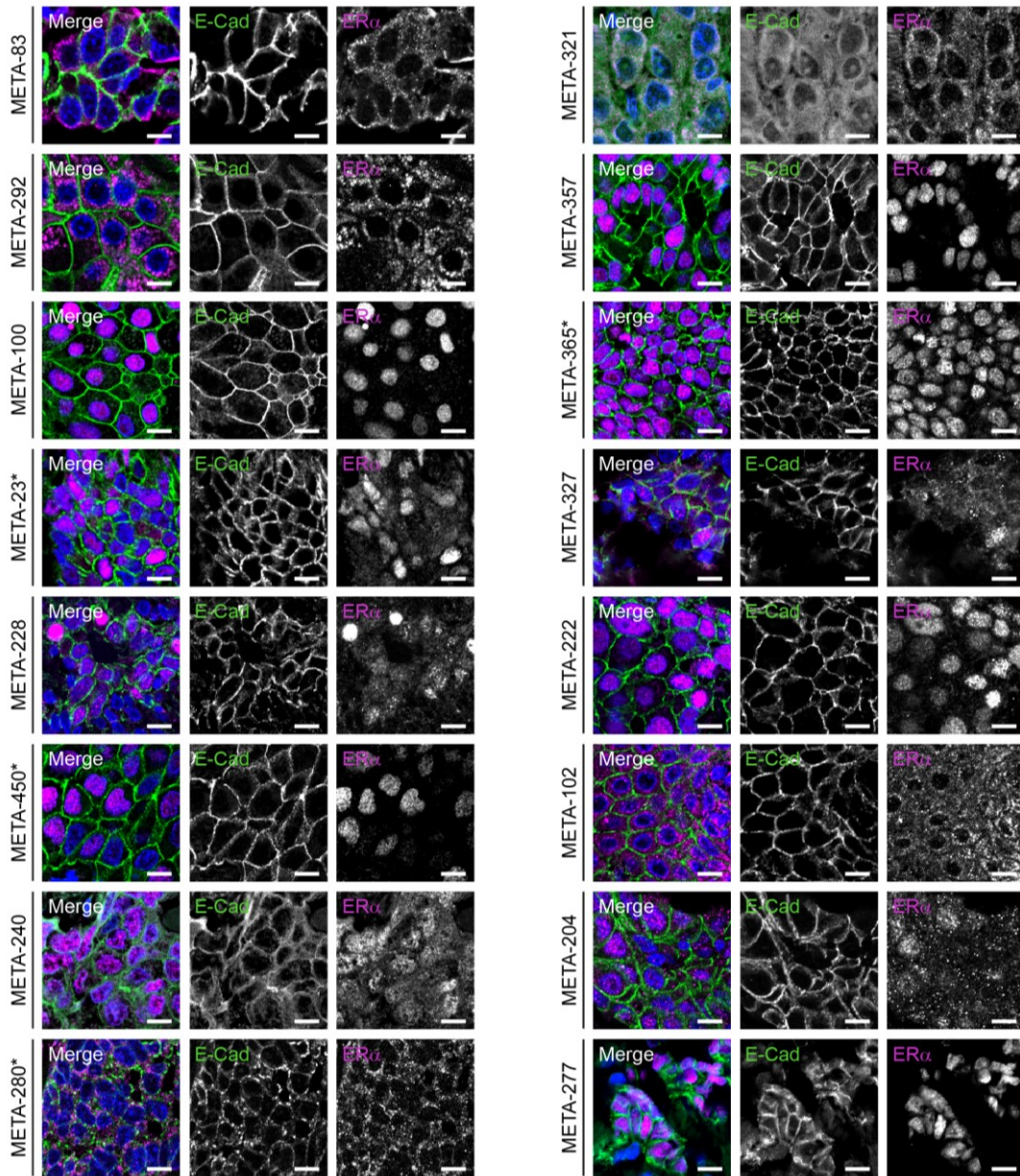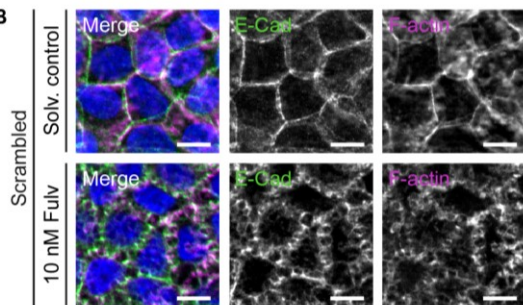Solv. control — Merge | E-Cad | F-actin
10 nM Fulv — Merge | E-Cad | F-actin

Figure S2 (Related to Figure 4 and Figure 5, Table 1 and Table 2) Adherens junction (AJ) organization and ERα localization in breast tumor tissue samples from METAcancer project.

(A) Immunofluorescence images showing AJ organization (E-Cad, green) and ERα localization (magenta) in breast tumor tissue samples from patients with diagnosed invasive ductal carcinoma (IDC). An asterisk indicates sections with clustered appearance of E-Cad along cell membranes. Samples obtained from METAcancer project (results summarized in table 1). The numbers of histological sections were anonymized. Scale bar, 10 µm.

(B) Control for experiment shown in Figure 4E. Immunofluorescence images showing E-Cad (green) and F-Actin (magenta) staining in Fulv-treated and solvent control-treated cells upon transfection with scrambled control siRNA for 48 hours. Scale bar, 10 µm.
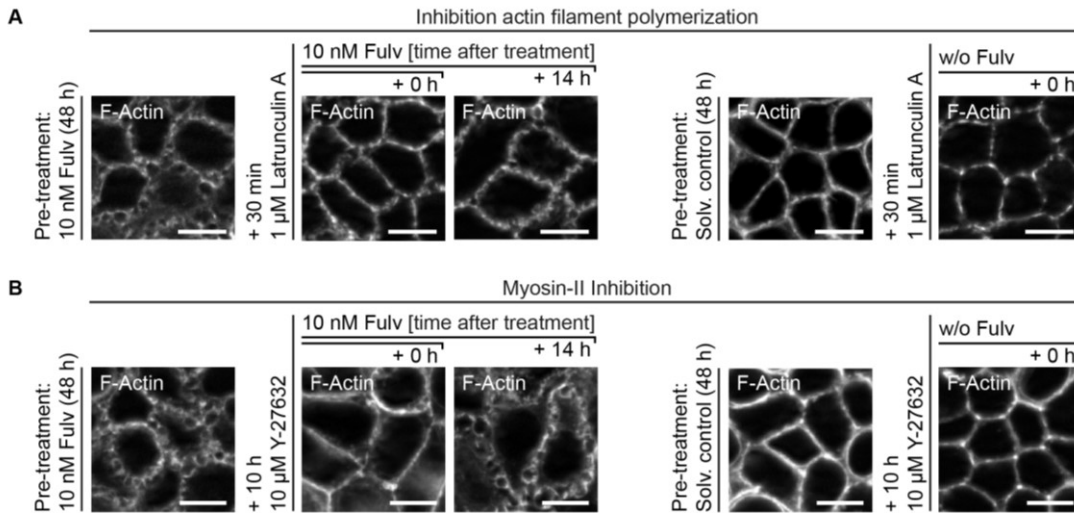
Figure S3 (Related to Figure 6) Adherens junction (AJ) organization upon modulation of the actomyosin cytoskeleton.

(A) F-Actin staining (proxy for AJ organization) of immunofluorescence images shown in figure 6A. Time points indicate time after removal of Latrunculin A-containing medium. Scale bar, 10 µm.

(B) F-Actin staining (proxy for AJ organization) of immunofluorescence images shown in figure 6B. Time points indicate time after removal of Y-27632-containing medium. Scale bar, 10 µm.

Transparent methods

Human cell line, cell culture, and drug treatments

MCF-7/vBOS (*Michigan Cancer Foundation-7/variantBOS*) cells used in this study originate from the MCF-7/BOS cell line (Soto and Sonnenschein, 1985) and its identity with regard to the ATCC MCF-7 reference cell line (HTB-22) was verified by the ATCC STR profiling service (ATCC). MCF-7/vBOS cells were deposited for patent purposes under the accession number *DSM ACC3321* at Leibniz Institute DSMZ-German Collection of Microorganisms and Cell Cultures. MCF7 cells stably expressing E-Cad-GFP (MCF-7/E-Cad-GFP) were described in (de Beco et al., 2009). HCT116 cells were obtained from ATCC.

Cell cultures were routinely maintained at 37 °C with 5 % CO_2 in normal-serum medium (Dulbecco's modified Eagle's medium (DMEM, Biochrom), 10 % (v/v) Fetal Bovine Serum (FBS, Biochrom, S0615, Estradiol levels: 18.6-22.3 pg/ml), 100 µg/ml streptomycin / 100 U/ml penicillin (Biochrom)). Cells were sub-cultured over a maximum of 8-10 passages, and regularly tested using the GATC mycoplasma test service (GATC Biotech).

All experiments were performed in reduced-serum medium (phenol red-free DMEM (Gibco), 5 % (v/v) FBS (Biochrom, S0615), 2 mM stable glutamine, 100 µg/ml streptomycin / 100 U/ml penicillin (Biochrom)). Depending on the experimental set-up, cells were grown in multi-well tissue culture microplates until 70-90 % confluency for 24 h and then treated for 48 h with Fulvestrant (Sigma-Aldrich/Tocris, CAS-No. 129453-61-8), (Z)-4-Hydroxytamoxifen (Tocris, CAS-No. 68047-06-3), Tamoxifen (Sigma-Aldrich, CAS-No. 10540-29-1), ZK164015 (Tocris, CAS-No. 177583-70-9), 17β-Estradiol (Sigma-Aldrich, CAS-No. 50-28-2) PHTPP (Tocris, CAS-No. 805239-56-9), Latrunculin A (Sigma-Aldrich, CAS-No: 76343-93-6), Y-27632 (Sigma-Aldrich, CAS-No: 129830-38-2), EGTA (CAS-No. 67-42-5, Roth), and Gefitinib (Tocris, CAS-No: 184475-35-2). Ethanol and Dimethyl Sulfoxide (DMSO) were used as solvent control at a final concentration of 0.1 % (v/v).

Transfection

Cells were transfected using HiPerFect Transfection Reagent (Qiagen) for siRNAs (10 nM) and FuGENE HD Transfection Reagent (Promega) or Torpedo DNA Transfection Reagent (Ibidi) for plasmids at 70-80 % confluency. siRNAs used: *ESR1*

(Qiagen, FlexiTube GeneSolution GS2099), *CDH1* (Qiagen, FlexiTube GeneSolution GS999), *AREG* (Qiagen, FlexiTube GeneSolution GS374), negative control (Qiagen, SI03650325). Plasmid used: pcDNA3.1-E-cadherin-GFP (Addgene, 28009) (Miranda et al., 2001), pCMV6-AREG-GFP (OriGene, RG203150), pSG5 empty vector (Green et al., 1988), pSG5-ERα/HEG0 (Tora et al., 1989), pSG5-ERβ (Cowley et al., 1997).

Quantitative RT-PCR

RNA extraction, cDNA synthesis, and quantitative RT-PCR reactions were performed applying the RNeasy Mini Kit (Qiagen), a Nanodrop 2000 spectrophotometer (Thermo Scientific), the High-Capacity cDNA Reverse Transcription Kit (Applied Biosystems), the PowerUp SYBR Green Master Mix (Applied Biosystems), and the QuantStudio 7 Real-time PCR system (Applied Biosystems). RNA expression levels (fold change) were calculated according to the $\Delta\Delta C_T$ method. Tyrosine 3-Monooxygenase/Tryptophan 5-Monooxygenase Activation Protein Zeta (YWHAZ) served as housekeeping gene (Chua et al., 2011). Primers used (5'-3' orientation):

BCL2L1 (CAGCTTGGATGGCCACTTAC, TGCTGCATTGTTCCCATAGA);
TFF1 (CATCGACGTCCCTCCAGAAGAG, CTCTGGGACTAATCACCGTGCTG);
PGR (TCAACTACCTGAGGCCGGAT, GCTCCCACAGGTAAGGACAC);
CDH1 (AGGAGCCAGACACATTTATGGAA, GCTGTGTACGTGCTGTTCTTCAC);
ESR1 (CCACCAACCAGTGCACCATT, GGTCTTTTCGTATCCCACCTTTC);
AREG (TGGATTGGACCTCAATGACA, TAGCCAGGTATTTGTGGTTCG);
YWHAZ (ACTTTTGGTACATTGTGGCTTCAA, CCGCCAGGACAAACCAGTAT).

Western blot

Cells were lysed in lysis buffer (50 mM Tris/HCl pH 7.4, 150 mM NaCl, 0.1 % (w/v) Na-deoxycholate, 0.1 % (w/v) SDS, 1 % (v/v) IGEPAL CA-630/NP-40, 5 mM EDTA pH 8.0, 5 mM EGTA, 1X cOmplete Protease Inhibitor Cocktail (Roche), PhosSTOP Phosphatase Inhibitor Cocktail (Roche) for 30 min on ice. Total protein concentration was determined using a Pierce BCA Protein Assay Kit (Thermo Scientific). Protein lysates were separated by SDS-PAGE. After protein transfer, nitrocellulose membranes were blocked with 5 % low-fat milk powder, and incubated with primary and secondary antibodies in 5 % low-fat milk powder in TBS-T (TBS, 0.1 % Tween 20) over night at 4°C and for 1 h at room temperature, respectively.

Antibodies/dyes used: anti-E-Cad (Clone 36, BD Biosciences); anti-E-Cad (G10, Santa Cruz); anti-E-Cad (H108, Santa Cruz); anti-ERα (F-10, Santa Cruz); anti-ERβ (1531, Santa Cruz); anti-Amphiregulin (16036-1-AP, Proteintech), and HRP-conjugated secondary antibodies (Santa Cruz). Protein detection was carried out using a SuperSignal West Femto Maximum Sensitivity Substrate (Thermo Scientific) in a Fusion Solo S (VWR) imaging system. Coomassie total protein staining of nitrocellulose membranes as loading control (Welinder and Ekblad, 2011) was quantified using the FIJI software (Schindelin et al., 2012).

Immunofluorescence microscopy

For immunofluorescence staining, cells were cultured as described above but seeded on glass coverslips in 12-well tissue culture microplates. For surface coating experiments, glass coverslips were coated with 0.5 µg/cm^2 fibronectin or 2 µg/cm^2 laminin (both Sigma-Aldrich) in PBS. After treatment, cells were fixed with 3. 7% formaldehyde in PBS for 15 min, permeabilized with 0.2 % Triton X-100 in PBS for 30 min, and blocked with 5 % FBS in PBS for 1 h at room temperature. Incubation with primary and secondary antibodies in PBS containing 1.5 % BSA was carried out over night at 4°C and for 1 h at room temperature, respectively. Antibodies/dyes used: anti-E-Cadherin (H-108, Santa Cruz); anti-E-Cadherin (G-10, Santa Cruz); anti-E-Cadherin (Clone 36, BD Biosciences); anti-α-Catenin (Abcam); anti-β-Catenin (BD Biosciences); anti-p120 (BD Biosciences); anti-ZO1 (Invitrogen); anti-ERα (HC-20, Santa Cruz); anti-ERα (F-10, Santa Cruz); fluorophore-conjugated Phalloidin (Sigma); DAPI (Roche); secondary antibodies conjugated to Cy2 (Jackson Immunoresearch), Cy3 (Jackson Immunoresearch), Alexa Fluor 488/555/647 (all Invitrogen). Samples were mounted in Dako fluorescence mounting medium (Dako) or VectaShield (Vector Labs). All images were acquired with an Axio Observer.Z1/Apotome.2, an LSM 510meta, or an LSM 880/Airyscan (all Zeiss). Images were analyzed using the FIJI software (Schindelin et al., 2012) and a CellProfiler/CellProfiler Analyst-based (Carpenter et al., 2006; Jones et al., 2008) image analysis pipeline as described below.

Live-cell fluorescence microscopy

MCF7/E-Cad-GFP cells were grown and treated in 96-well glass bottom ViewPlate microplates (PerkinElmer) as described above for 24 h. Prior to imaging, cells were stained with 20 µg/ml Hoechst 33342 (Molecular Probes) in medium and

imaged every 2 h for 24 h at 37 °C with 5 % CO_2 using an Opera Phenix high-content screening system (PerkinElmer). The resulting time-resolved image stacks (technical replicates from 3 wells, 9 positions per well, 16 optical z-sections per position, step size 1 µm) were subsequently analyzed as maximum projections of all optical sections using the integrated Harmony software as described below.

Quantitative image analysis

Customized image analysis pipelines have been generated using the CellProfiler (Carpenter et al., 2006) and CellProfiler Analyst (Jones et al., 2008) software packages and are available upon request. For analyses of adherens junction organization, the image analysis pipeline included *i)* an image segmentation step to generate segmentation masks of cell membranes for extraction of cellular parameters, and *ii)* a parameter-based classification step to sort cells into two categories, i.e. 'Continuous AJs' and 'Discontinuous AJs', by supervised machine learning. During the CellProfiler-based image segmentation process, primary objects (nuclei) were identified from the DAPI channel by global thresholding (*PrimaryObjects* module, Otsu method). After automatic exclusion of primary objects with an area smaller than 1000 pixels, the segmentation masks of the nuclei were checked and, if necessary, manually corrected using the *EditOjectsManually* module. These primary objects then served as seeding points for the identification of secondary objects (cells) from the E-Cad channel (*SecondaryObjects* module, watershed-gradient method), followed by automatic exclusion of objects touching the image border (border objects) and secondary objects with an area greater than 8000 pixels (clumped objects). Finally, tertiary objects (cell membranes) were defined by shrinking secondary objects by three pixels (*TertiaryObjects* module). Based on the resulting cell membrane segmentation masks, cellular parameters (distribution and variation of pixel intensities) were extracted from the corresponding E-Cad channel using the *MeasureTexture* module and exported into a relational database along with a CellProfiler Analyst properties file. During the CellProfiler Analyst-based image classification process, the *Classifier* module was manually trained with cells that were randomly selected from positive (Fulv treatment) and negative control (solvent) images to define the cellular parameters underlying the two categories 'Continuous AJs' and 'Discontinuous AJs' (50 cells per class) by supervised machine learning. This training set was then applied to classify all cells from the entire image dataset of each individual experiment using the Random

Forest classifier model, and the enrichment or depletion of each class was calculated per image.

The Image analysis of the quantitative calcium switch assay only slightly deviated from the pipeline described above. Primary objects (nuclei) were identified from the Hoechst 33342 channel by global thresholding using Otsu's method. Secondary objects (cells) were identified using the Distance-B method from the CellTrace Far Red channel. Cellular parameters were extracted from the corresponding CellTrace Far Red channel using the *MeasureObjectRadialDistribution*, *MeasureObjectSizeShape*, *MeasureTexture*, *MeasureGranularity* modules. Supervised machine learning was conducted as described above to define the cellular parameters underlying the two categories 'Rounded cells' and 'Non-rounded cells' (50 cells per class).

The image analysis of the live-cell imaging of MCF7/E-Cad-GFP cells was performed using the Harmony image analysis software (PerkinElmer) following the same principle as described for the CellProfiler/CellProfiler Analyst pipeline. Upon segmentation of nuclei (*FindNuclei* module, method C, Hoechst 33342 channel), identification of the cytoplasm (*FindCytoplasm* module, method A, GFP channel), and exclusion of the cells at the edges of the image (*SelectPopulation* module), cellular parameters were extracted using the *CalculateMorphologyProperties* module with activated STAR features (threshold compactness and profile). For cell classification, supervised machine learning was conducted as described above using cells randomly selected from positive control (Fulv treatment) and negative control (solvent) images of the final timepoint (*SelectPopulation* module, Linear Classifier method) to define the cellular parameters underlying the two categories 'Continuous AJs' and 'Discontinuous AJs' (50 cells per class).

All image analyses have been performed on three individual images from each condition in three biological replicates, if not otherwise stated.

Breast tumor tissue samples

Formalin-fixed paraffin-embedded breast tumor tissue samples that were collected in the context of the METAcancer consortium (Denkert et al., 2012) and the ADAPT clinical trial (Hofmann et al., 2013) were provided by Carsten Denkert (Institute of Pathology, UKGM Gießen/Marburg, Germany) and prepared for immunofluorescence microscopy according to Junghans et al. (2005). Tissue sections

were subjected to immunofluorescence staining, imaging, and image analysis as described for the cell culture experiments.

Transmission electron microscopy (TEM)

For TEM analysis, cells were grown and treated as described above but seeded on ACLAR Fluoropolymer-Film (Science Services). For conventional TEM, cells were fixed with 2.5 % glutaraldehyde in PBS/reduced-serum medium (1:1, v/v) for 1 h, post-fixed with 0.5 % osmium tetroxide in PBS for 1 h, and incubated with 0.1 % tannic acid in PBS for 30 min at room temperature. After contrasting with 2 % uranyl acetate in PBS for 1.5 h, cells were dehydrated in serial dilutions of ethanol in water at room temperature. Samples were embedded in Spurr's resin using a Low Viscosity "Spurr" Kit (Ted Pella), polymerized for 3 d at 60 °C, and finally subjected to ultrathin sectioning and TEM.

For immuno-TEM, cells were fixed with 4 % paraformaldehyde / 0.2 % glutaraldehyde in PBS/reduced-serum medium (1:1, v/v) for 30 min, incubated with 0.1 % tannic acid in PBS for 30 min, and dehydrated in serial dilutions of ethanol in PBS at room temperature. Samples were embedded in LR-Gold resin (Plano, Wetzlar), polymerized under a 100 W UV lamp for 2 d at 4°C, and subjected to ultrathin sectioning. Ultrathin 80 nm sections were blocked with 0.4 % BSA in 20 mM Tris / 0.015 M NaCl for 30 min at room temperature, and stained with primary and secondary antibodies in 0.4 % BSA in 20 mM Tris / 0.015 M NaCl over night at 4 °C and for 2 h at room temperature, respectively. Antibodies used: anti-E-Cadherin (H-108, Santa Cruz); secondary antibody conjugated to Au10 (BBI Solutions). After contrasting with 2 % uranyl acetate in PBS for 2 min and lead citrate for 1 min at room temperature, samples were subjected to TEM. All images were acquired with a Tecnai Spirit Transmission Electron Microscope (FEI) operated at 120 kV, which was equipped with a F416 CMOS 4kx4k camera (TVIPS). Micrographs were automatically recorded using the Leginon system (Suloway et al., 2005) and stitched using the TrakEM2 (Cardona et al., 2012) FIJI plugin.

Atomic force microscopy (AFM) indentation measurements

Cells were grown and treated in 35 mm FluoroDish cell culture dishes (WPI) as described above. AFM indentation measurements were performed in CO_2 Independent Medium (Gibco) at 37 °C using the NanoWizard 1 or 4 (JPK Instruments). Prior to

measurements, tip-less Arrow-TL1silicone cantilevers (Nanoworld) were equipped with polystyrene beads of 5 μm in diameter (microParticles GmbH) using epoxy glue, and calibrated using built-in procedures of the SPM software (JPK Instruments). The cantilever was positioned above the confluent cellular monolayer and lowered with a speed of 10 μm/s. In each experiment, force-distance curves (force setpoint 2.5 nN) from 3-4 different positions per cell were collected. Force-distance curves were transformed into force-versus-tip sample separation curves according to Radmacher (2002), and fitted with the Hertz/Sneddon model (Sneddon, 1965) for a spherical indenter using the JPK Data Processing software (JPK Instruments). A Poisson ratio of 0.5 was assumed for the calculation of the apparent elastic (Young's) modulus. To map the elastic modulus distribution, cells were probed with a spatial resolution of 1 μm using a MLCT cantilever (Bruker). Apparent elastic (Young's) moduli were determined using the Hertz model for a quadratic pyramid using the JPK Data Processing software (JPK Instruments).

Trypsin assay

Cells were grown and treated in 6-well tissue culture plates as described above for 48 h. Following, cells were washed with PBS and incubated in Trypsin/EDTA (0.05 % / 0.02 %) (Biochrom) for 4 min at 37 °C. The supernatant was collected for protein extraction and western blot analysis as described above.

Calcium switch assay

Cells were grown and treated in 96-well glass bottom ViewPlate microplates (PerkinElmer) as described above, stained with 10 μM CellTrace Far Red and 1 μg/ml Hoechst 33342 (both Molecular Probes) in PBS for 20 min, washed two times with medium, and further incubated for 10 min at 37 °C with 5 % CO_2. Upon addition of EGTA, cells were immediately imaged using an Opera Phenix High Content Screening System (PerkinElmer) over the course of time. The resulting time stacks were analyzed using a CellProfiler/CellProfiler Analyst-based (Carpenter et al., 2006; Jones et al., 2008) image analysis pipeline as described above.

Cell motility assay

Cells were grown and treated in 12-well tissue culture plates as described above. Upon addition of 10 μM Cytarabine (CAS-No. 147-94-4, Sigma-Aldrich) to

inhibit cell proliferation, the cell monolayer was scraped in a straight line. Confluent cells close to the scratch were recorded by phase contrast microscopy. For image analysis, a total of 30 cells from three individual areas (10 cells per area) were tracked every 10 minutes over the course of 16 hours using Fiji plugins. Manual tracking of cells, calculation of cell velocity, and plotting of cell trajectories was performed using the MTrackJ (Meijering et al., 2012) and Chemotaxis and Migration Tool (Ibidi) plugins for FIJI.

Statistical analysis

Graphical visualization and statistical analysis of data was performed using the GraphPad Prism software. Figures were generated using Adobe Illustrator.

Supplemental references

Cardona, A., Saalfeld, S., Schindelin, J., Arganda-Carreras, I., Preibisch, S., Longair, M., Tomancak, P., Hartenstein, V., and Douglas, R.J. (2012). TrakEM2 software for neural circuit reconstruction. PLoS One *7*, e38011.

Carpenter, A.E., Jones, T.R., Lamprecht, M.R., Clarke, C., Kang, I.H., Friman, O., Guertin, D.A., Chang, J.H., Lindquist, R.A., Moffat, J.*, et al.* (2006). CellProfiler: image analysis software for identifying and quantifying cell phenotypes. Genome Biol *7*, R100.

Chua, S.L., See Too, W.C., Khoo, B.Y., and Few, L.L. (2011). UBC and YWHAZ as suitable reference genes for accurate normalisation of gene expression using MCF7, HCT116 and HepG2 cell lines. Cytotechnology *63*, 645-654.

Cowley, S.M., Hoare, S., Mosselman, S., and Parker, M.G. (1997). Estrogen receptors alpha and beta form heterodimers on DNA. The Journal of biological chemistry *272*, 19858-19862.

de Beco, S., Gueudry, C., Amblard, F., and Coscoy, S. (2009). Endocytosis is required for E-cadherin redistribution at mature adherens junctions. Proc Natl Acad Sci U S A *106*, 7010-7015.

Denkert, C., Bucher, E., Hilvo, M., Salek, R., Oresic, M., Griffin, J., Brockmoller, S., Klauschen, F., Loibl, S., Barupal, D.K.*, et al.* (2012). Metabolomics of human breast cancer: new approaches for tumor typing and biomarker discovery. Genome Med *4*, 37.

Green, S., Issemann, I., and Sheer, E. (1988). A versatile in vivo and in vitro eukaryotic expression vector for protein engineering. Nucleic Acids Res *16*, 369.

Hofmann, D., Nitz, U., Gluz, O., Kates, R.E., Schinkoethe, T., Staib, P., and Harbeck, N. (2013). WSG ADAPT - adjuvant dynamic marker-adjusted personalized therapy trial optimizing risk assessment and therapy response prediction in early breast cancer: study protocol for a prospective, multi-center, controlled, non-blinded, randomized, investigator initiated phase II/III trial. Trials *14*, 261.

Jones, T.R., Kang, I.H., Wheeler, D.B., Lindquist, R.A., Papallo, A., Sabatini, D.M., Golland, P., and Carpenter, A.E. (2008). CellProfiler Analyst: data exploration and analysis software for complex image-based screens. BMC Bioinformatics *9*, 482.

Junghans, D., Hack, I., Frotscher, M., Taylor, V., and Kemler, R. (2005). Beta-catenin-mediated cell-adhesion is vital for embryonic forebrain development. Dev Dyn *233*, 528-539.

Meijering, E., Dzyubachyk, O., and Smal, I. (2012). Methods for cell and particle tracking. Methods Enzymol *504*, 183-200.

Miranda, K.C., Khromykh, T., Christy, P., Le, T.L., Gottardi, C.J., Yap, A.S., Stow, J.L., and Teasdale, R.D. (2001). A dileucine motif targets E-cadherin to the basolateral cell surface in Madin-Darby canine kidney and LLC-PK1 epithelial cells. J Biol Chem *276*, 22565-22572.

Radmacher, M. (2002). Measuring the elastic properties of living cells by the atomic force microscope. Methods Cell Biol *68*, 67-90.

Schindelin, J., Arganda-Carreras, I., Frise, E., Kaynig, V., Longair, M., Pietzsch, T., Preibisch, S., Rueden, C., Saalfeld, S., Schmid, B.*, et al.* (2012). Fiji: an open-source platform for biological-image analysis. Nat Methods *9*, 676-682.

Sneddon, I.N. (1965). The relation between load and penetration in the axisymmetric boussinesq problem for a punch of arbitrary profile. International Journal of Engineering Science *3*, 47-57.

Soto, A.M., and Sonnenschein, C. (1985). The role of estrogens on the proliferation of human breast tumor cells (MCF-7). J Steroid Biochem *23*, 87-94.

Suloway, C., Pulokas, J., Fellmann, D., Cheng, A., Guerra, F., Quispe, J., Stagg, S., Potter, C.S., and Carragher, B. (2005). Automated molecular microscopy: the new Leginon system. J Struct Biol *151*, 41-60.

Tora, L., Mullick, A., Metzger, D., Ponglikitmongkol, M., Park, I., and Chambon, P. (1989). The cloned human oestrogen receptor contains a mutation which alters its hormone binding properties. EMBO J *8*, 1981-1986.

Welinder, C., and Ekblad, L. (2011). Coomassie staining as loading control in Western blot analysis. J Proteome Res *10*, 1416-1419.